

The coupled atmosphere-ocean response to Antarctic sea-ice loss

Article

Accepted Version

Ayres, H. C. ORCID: <https://orcid.org/0000-0003-0294-7620>, Screen, J. A., Blockley, E. W. and Bracegirdle, T. J. (2022) The coupled atmosphere-ocean response to Antarctic sea-ice loss. *Journal of Climate*, 35 (14). pp. 4665-4685. ISSN 1520-0442 doi: <https://doi.org/10.1175/JCLI-D-21-0918.1> Available at <https://centaur.reading.ac.uk/104573/>

It is advisable to refer to the publisher's version if you intend to cite from the work. See [Guidance on citing](#).

To link to this article DOI: <http://dx.doi.org/10.1175/JCLI-D-21-0918.1>

Publisher: American Meteorological Society

All outputs in CentAUR are protected by Intellectual Property Rights law, including copyright law. Copyright and IPR is retained by the creators or other copyright holders. Terms and conditions for use of this material are defined in the [End User Agreement](#).

www.reading.ac.uk/centaur

CentAUR

Central Archive at the University of Reading

Reading's research outputs online



1
2
3
4
5
6
7
8
9
10
11
12
13

The coupled atmosphere-ocean response to Antarctic sea-ice loss

Holly C. Ayres,^{a,b} James A. Screen,^b Edward W. Blockley,^c Thomas J. Bracegirdle^d.

^a *Department of Meteorology, University of Reading, Reading, UK*

^b *College of Engineering, Mathematics and Physical Sciences, University of Exeter, Exeter, UK*

^c *Met Office Hadley Centre, Met Office, Exeter, UK*

^d *British Antarctic Survey, Cambridge, UK*

Corresponding author: Holly C Ayres, h.c.ayres@reading.ac.uk

14 ABSTRACT

15 Antarctic sea ice is projected to decrease in response to increasing greenhouse gas
16 concentrations. Limited studies so far have examined the coupled atmosphere-ocean response
17 to Antarctic sea-ice loss. Here, we isolate the response to Antarctic sea-ice loss in the
18 atmosphere and ocean using bespoke sea-ice albedo perturbation experiments with HadGEM3-
19 GC31-LL, provide the first detailed examination of the global ocean response, and quantify the
20 importance of atmosphere-ocean coupling, through comparison to uncoupled experiments with
21 prescribed Antarctic sea-ice loss. Lower tropospheric warming and moistening over regions of
22 sea-ice loss and the nearby Southern Ocean are simulated in both coupled and uncoupled
23 configurations but are of greater magnitude in the coupled model. A weakening and
24 equatorward shift of the tropospheric westerly jet are simulated in both configurations, but are
25 also larger in the coupled model. Ocean coupling allows the warming response to spread
26 northward, and by poleward atmospheric energy transport, back to the Antarctic interior.
27 Warmer tropical sea surface temperatures enhance atmospheric convection, driving upper-
28 tropospheric warming and triggering atmospheric teleconnections to the extratropics, including
29 a weakened Aleutian Low. A 20% reduction in Antarctic Circumpolar Current transport and a
30 weakening of the shallow tropical convergence cell are simulated. Surface waters warm and
31 freshen globally, becoming more stratified and stable in the Southern Ocean, with similar
32 changes, but of lesser magnitude, in the Arctic Ocean, where sea ice declines. Our results
33 suggest that the climate effects of Antarctic sea-ice loss stretch from pole-to-pole and from the
34 heights of the tropical troposphere to the depths of the Southern Ocean.

35

36 **1. Introduction**

37 Over the modern satellite era, from 1979 to 2018, annual-mean Antarctic sea ice extent
38 (SIE) increased, on average, by 11 thousand square kilometres per year (Parkinson, 2019). This
39 counterintuitive increase, in a warming world, contrasts with the large decline in the Arctic,
40 and the decline simulated for the Antarctic in models over the historical period (e.g., Meredith
41 et al., 2019). Many possible explanations for observed increase of Antarctic sea ice cover, and
42 the failure of models to reproduce it, have been suggested, including, but not limited to, internal
43 climate variability (Singh et al., 2019), stratospheric ozone depletion (Turner et al., 2009;

44 Polvani et al., 2011), and surface freshening due to enhanced precipitation (Liu and Curry
45 2010) or glacial meltwater (Bintanja et al., 2013; Mackie et al., 2020).

46 The observed trend of increasing sea ice has become weaker in recent years, and is no
47 longer statistically significant (Parkinson, 2019), after the previous record low SIE in austral
48 winter 2016 (Turner et al., 2017), in addition to a new record low in austral winter 2022
49 (Raphael & Handcock, 2022). Possible explanations for the sudden 2016 decline include
50 influences from ENSO and an enhanced zonal wavenumber-3 pattern of the westerly jet
51 (Schlosser et al., 2017; Stuecker et al., 2017), a rare stratospheric warming event that
52 subsequently influenced the westerly jet and enhanced ice melt (Meehl et al., 2019; Wang et
53 al., 2019), and the unprecedented opening of a polynya near the Maude Rise (Turner et al.,
54 2020). It is unclear if this substantial reduction is temporary or if the Antarctic sea ice is
55 entering a new era of decline (Ludescher et al., 2018; Eayrs et al., 2021). Regardless, models
56 project Antarctic sea-ice loss over this century in response to increasing greenhouse gas
57 concentrations (Collins et al., 2013; Roach et al., 2020).

58 The climate response to Arctic sea-ice loss has been well studied (e.g., Blackport &
59 Kushner, 2016; Blackport & Screen, 2020; Cohen et al., 2014; Deser et al., 2015; Kim et al.,
60 2014; Peings & Magnusdottir, 2014; Screen et al., 2018; Screen & Simmonds, 2013; Screen et
61 al., 2013; Vavrus, 2018; Zappa et al., 2018). By comparison however, only a handful of
62 modelling studies have been conducted on the impacts of Antarctic sea-ice loss. Model studies
63 forced by observed sea ice trends suggest that the growth in Antarctic sea ice results in a slight
64 poleward shift of the tropospheric eddy-driven jet and a positive Southern Annular Mode
65 (SAM) anomaly in winter months (Raphael et al., 2011; Smith et al., 2017). Modelling studies,
66 using atmosphere-only model configurations prescribed with projected Antarctic sea-ice loss,
67 have found contrasting results on the impact on the location of the mid-latitude tropospheric
68 eddy-driven jet, but generally agree that there is a reduction in its strength (Bader et al., 2013;
69 England et al., 2018; Kidston et al., 2011; Menéndez et al., 1999). In addition to the impacts
70 on the jet, England et al. (2018) found that the responses to Antarctic sea-ice loss were more
71 vertically confined, of smaller amplitude, and less seasonally variable than the well-studied
72 response to Arctic sea-ice loss.

73 Ayres and Screen (2019) provided the first multi-model analysis of the atmospheric
74 response to projected Antarctic sea-ice loss, indirectly inferred from the Coupled Model
75 Intercomparison Project phase 5 (CMIP5) ensemble (Taylor et al., 2012). Antarctic sea-ice loss

76 caused a robust weakening of the tropospheric westerly jet and favoured the negative phase of
77 the SAM, of greatest magnitude and robustness in spring and summer. In these regards, the
78 response to sea-ice loss acts to weakly damp the strengthening westerly jet and positive SAM
79 responses to increased CO₂. The SAM response to sea-ice loss primarily reflected a reduction
80 in jet strength and to a lesser extent, an equatorward shift in the jet. In spring, this study found
81 multi-model evidence for a weakening polar stratospheric vortex and coupling between the
82 stratospheric and tropospheric zonal wind responses. Sea-ice loss induced warming in the
83 lowermost atmosphere over the high-latitude Southern Ocean, but this warming did not
84 penetrate over the Antarctic continent, consistent with England et al. (2018).

85 The majority of the above-mentioned studies used atmosphere-only models, as opposed to
86 fully coupled atmosphere-ocean models, which may lead to muted responses, or in the case of
87 Ayres and Screen (2019), used an indirect method that may miss aspects of the remote
88 response. An important role of ocean coupling in the atmospheric response to Arctic sea-ice
89 loss has been established (Deser et al., 2016; Smith et al., 2017; Tomas et al., 2016).
90 Atmosphere-only models depict locally confined changes in response to Arctic sea-ice loss, as
91 far south as the mid-latitudes, whereas coupled models suggest more widespread effects,
92 reaching the tropics and even into the Southern Hemisphere (e.g., Blackport and Kushner 2016;
93 Deser et al., 2016, 2015; Oudar et al., 2017).

94 Much less is known about the importance of ocean-atmosphere coupling for the response
95 to Antarctic sea-ice loss. England et al., (2020a) was the first study to use a coupled climate
96 model to assess the impact of Antarctic sea-ice loss and showed that ocean dynamics are
97 important in capturing the global response to Antarctic sea-ice loss, just as is the case for the
98 response to Arctic sea-ice loss. These authors found that the tropical response to Antarctic sea-
99 ice loss is like that to Arctic sea-ice loss, particularly in the eastern equatorial Pacific. Antarctic
100 sea-ice loss induced a ‘mini global warming’ signal, having a spatial pattern like that seen in
101 response to increased greenhouse gas concentrations, but with smaller magnitude (this ‘mini
102 global warming’ pattern has also been found in coupled models forced by projected Arctic sea-
103 ice loss). Arctic warming in response to Antarctic sea-ice loss, was induced through changes
104 in tropical Pacific Ocean and associated atmospheric teleconnections to the Aleutian Low
105 (England et al., 2020b). The above two studies suggest that the ocean may play an important
106 role in the climate response to Antarctic sea-ice loss. Yet, the impact of Antarctic sea-ice loss
107 on the ocean has not been assessed in any detail.

108 Here, we advance the science on the climate response to Antarctic sea-ice loss in three main
109 ways. First, we use a novel coupled modelling framework to isolate the atmospheric response
110 to Antarctic sea-ice loss in the coupled climate system, building on the work of England et al.
111 (2020a; 2020b), and assess the local and global effects. Second, we provide the first detailed
112 examination of the oceanic response to Antarctic sea-ice loss (Section 3f - h). Third, by
113 contrasting analogous coupled and uncoupled experiments, we provide the clearest yet
114 determination of the role of the ocean and atmosphere-ocean coupling in the climate response
115 to Antarctic sea-ice loss.

116

117 **2. Methods**

118 *a. Model configurations*

119 The bespoke sea ice perturbation experiments use the HadGEM3-GC3.1-LL low resolution
120 (N96-ORCA1) global coupled model configuration, which participated in phase 6 of the CMIP
121 (Williams et al., 2017). The model uses the MetUM GA7.1 global atmosphere and JULES
122 GL7.0 land surface configurations (Walters et al. 2017), coupled to the NEMO GO6.0 ocean
123 (Storkey et al., 2018), and CICE GSI8.1 sea ice (Ridley et al., 2018) model configurations.
124 This version has an atmosphere with 85 vertical levels and horizontal resolution of ~135 km at
125 mid-latitudes (N96). The ocean model used has 75 vertical levels with a 1° horizontal resolution
126 on a tripolar grid. An advantage of using the N96-ORCA1 model over the N216-ORCA025
127 model, is that it requires an order of magnitude less computing power per model year, yet
128 maintains almost the same quality in representation of the global climate (Kuhlbrodt et al.,
129 2018), and, for this study in particular, performs better for Antarctic sea ice (Andrews et al.,
130 2020). The 1° ocean resolution requires a parameterization for eddy-induced transports
131 (Kuhlbrodt et al., 2018; Storkey et al., 2018), which here is a globally uniform coefficient. For
132 the atmosphere-only experiments, the same atmosphere and land component models are used,
133 but are not coupled to either an ocean or sea ice component model, as discussed in section 3c.

134 *b. Coupled experiments*

135 The control experiment was the CMIP6 ‘Preindustrial Control’ simulation (Eyring et al.
136 2016) of HadGEM3-GC3.1-LL, which was spun-up using CMIP6 Preindustrial forcing
137 (Menary et al., 2018). The version of HadGEM3 used here includes the impact of melt ponds;

138 ponds are evolved within the sea ice component but only used within the albedo scheme. In the
 139 sea ice perturbation experiment, sea-ice loss was induced in the Southern Hemisphere alone,
 140 via an albedo perturbation method. More specifically, all sea ice in the Southern Hemisphere
 141 was set to have the albedo of a melt pond with 30 cm depth. This perturbation caused an abrupt
 142 reduction in sea ice albedo, leading to the increased absorption of shortwave radiation and thus,
 143 abrupt Antarctic sea-ice loss. All other forcings were kept constant at preindustrial levels.
 144 Although melt ponds are naturally rare in the Antarctic due to thick snow cover (Scott and
 145 Feltham 2010), modifying the melt pond scheme was an effective way to control the sea ice in
 146 one hemisphere and not the other. All the parameters used within the albedo scheme, i.e., melt-
 147 ponds, bare sea ice, and snow, remain globally consistent and unchanged from the control
 148 experiment. We use the fact that the albedo of melt-ponds is lower than ice and snow to reduce
 149 the total albedo of the sea ice.

150 Within HadGEM3 the total albedo of the sea ice is calculated, separately for both visible
 151 (< 700 nm) and near-infrared (> 700 nm) wavelengths, as a combination of the albedos of bare
 152 ice, snow and melt pond using the CCSM3 scheme (Ridley et al., 2018). The evolution of melt
 153 pond area fraction, $f_p(n)$, and depth, $h_p(n)$, for ice in thickness category n , are calculated in
 154 CICE using the topographic melt pond formulation (Flocco et al., 2010; Hunke et al., 2015).
 155 This melt pond scheme includes the evolution of refrozen lids (Flocco et al., 2010), the impact
 156 of which are included by using the ‘effective pond fraction’ within the albedo calculations.
 157 When pond depth is less than 4mm, the melt pond has no impact on the albedo for that ice
 158 thickness category n , such that the ponded ice albedo is equal to that of bare ice, α_i . Conversely,
 159 where melt pond depth is greater than 20 cm, the bare ice albedo has no impact, and the ponded
 160 ice albedo is equal to that of a melt pond, α_p . For melt pond depths between these two values,
 161 the ponded ice albedo is a function of the underlying bare ice albedo and the pond albedo
 162 (Ridley et al., 2018; Briegleb & Light, 2007):

$$163 \quad \alpha_{pi}(n) = \frac{h_p(n)}{0.2} \alpha_p + \left(1 - \frac{h_p(n)}{0.2}\right) \alpha_i \quad (1)$$

164 The total grid-box albedo, $\alpha(n)$, of each sea ice thickness category n , is calculated as the
 165 combined ponded ice albedo, $\alpha_{pi}(n)$, bare ice albedo $\alpha_i(n)$, and snow albedo, $\alpha_s(n)$, weighted
 166 by the melt pond fraction $f_p(n)$ and snow fraction $f_s(n)$:

$$167 \quad \alpha(n) = f_p(n) \alpha_{pi}(n) + \left(1 - f_p(n)\right) \times \left(f_s(n) \alpha_s(n) + \left(1 - f_s(n)\right) \alpha_i\right) \quad (2)$$

168 Equation (2) dictates that when the melt pond fraction is one, the total albedo is solely
169 dependent on the ponded ice albedo, whereas when melt pond fraction is zero, the total albedo
170 is solely dependent on the snow albedo and bare ice albedo. For the purposes of this work, the
171 melt pond fraction and depth used within the albedo scheme were set to constant values F_p and
172 H_p , imposed as additional model parameters, to control the albedo of the sea ice.

173 Various combinations of F_p and H_p were tested in short sensitivity experiments, which
174 yielded varying magnitudes of sea-ice loss. Here, we present results using $F_p = 1$ and $H_p = 30$
175 cm. This parameter set resulted in the largest sea ice loss and was chosen to maximise the
176 signal-to-noise ratio and because it gave magnitudes of winter sea-ice loss to be closer to that
177 projected at the end of the twenty-first century (Roach et al., 2020). This forcing was applied
178 continually in a 300-year perturbation simulation, sufficiently long to allow the ocean
179 circulation to reach a new quasi-equilibrium state (Deser et al., 2016).

180 *c. Atmosphere-only experiments*

181 In the uncoupled control simulation, both the prescribed sea ice concentrations and sea
182 surface temperatures were taken from the coupled control simulation, averaged over years 50-
183 300. In the uncoupled sea ice perturbation experiment, sea ice concentrations in the Southern
184 Hemisphere were taken from the coupled albedo perturbation experiment, averaged over years
185 50-300, whilst those in the Northern Hemisphere were taken from the coupled control
186 simulation. Sea surface temperatures were set to the values from coupled albedo perturbation
187 experiment over regions of Antarctic sea-ice loss, but to the values from the coupled control
188 simulations elsewhere. All external forcings were kept constant at preindustrial levels.

189 The atmosphere-only simulation were run following the Polar Amplification Model
190 Intercomparison Project protocol (Smith et al., 2018). More specifically, the model was run for
191 14 months, starting 1st April, with a total of 200 members, whereby the initial conditions are
192 the same, but differ in the initial seed for the stochastic physics scheme. The first 2 months of
193 each run were discarded, and the remaining 200 years averaged to minimise the impact of
194 internal variability.

195 *d. Diagnostics and statistics*

196 Quasi-equilibrated responses were estimated by subtracting the time-mean in the control
197 simulation from that in the perturbation simulation, each comprising 250 years in the coupled

198 experiments and 200-year ensemble mean in the atmosphere-only experiments. Transient
199 responses in the coupled experiment were estimated by subtracting the control from the
200 perturbation at each time step. The statistical significance of the response (i.e., the difference
201 in means between the control and perturbation experiments) was calculated with the Student's
202 t-test and is reported at the 95% confidence level. All figures display only significant results.

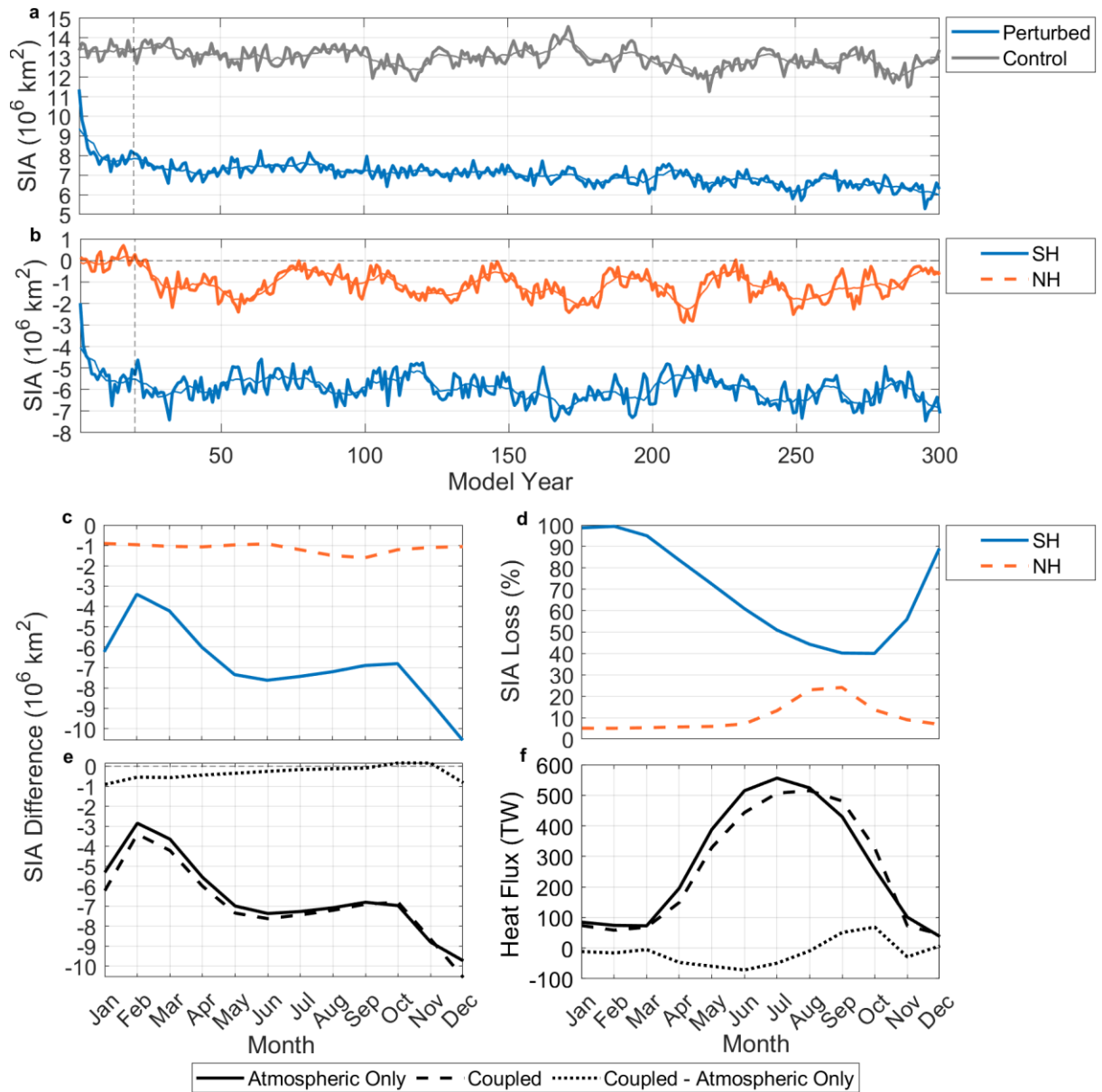
203 The mid-latitude tropospheric eddy-driven jet was characterised in terms of its strength (the
204 maximum velocity) and latitude, following the methodology used by Ceppi et al. (2018), Zappa
205 et al. (2018) and Ayres and Screen (2019). The Antarctic Circumpolar Current (ACC) volume
206 transport was calculated as the vertically integrated volume transport across Drake Passage
207 (54.5– 61 °S, 61 °W). Sea ice area was calculated by multiplying the sea ice fraction of each
208 grid cell by the true area of each grid cell, and summing over the hemisphere of interest, and
209 has units of (million) square kilometres.

210

211 **3. Results**

212 *a. Sea ice and surface fluxes*

213 Annual-mean Antarctic sea ice area (SIA) is around 13 million km² in the coupled control
214 simulation, with a small downward drift over time (Figure 1a). Following the albedo
215 perturbation, SIA decreases to around 8 million km² in year 5, and then to around 7 million
216 km² by year 20. After this, SIA continues to decrease slowly to 6 million km² in year 300. After
217 approximately year 20, the control and perturbed simulation show similar slow rates of decline,
218 such that the anomaly (perturbation minus control) remains fairly level at -6 million km² from
219 year 20 to 300, but with interannual and (multi-)decadal variability (Figure 1b). The coupled
220 perturbed simulation exhibits a complete loss of sea ice in summer and a 40% loss in SIA in
221 winter, relative to the preindustrial control state (Figure 1c). The seasonal cycle of SIA loss in
222 real terms (i.e., in square kilometres) is largest in early summer, when the effect of the albedo
223 change is largest, owing to maximum incoming solar radiation, and smallest in late summer,
224 when there is little sea ice in the control run anyway (Figure 1d). The annual-mean sea-ice loss
225 is broadly comparable to that projected in the high emission scenarios by the end of the 21st
226 century, albeit with greater ice loss in the summer and lesser ice loss in winter (not shown).



227

228 **Figure 1.** Time-series of Antarctic sea ice area in the coupled control and albedo
 229 perturbation experiments (grey and blue, respectively). The thin curves show 10-year running
 230 means. The dashed vertical line shows the end of the spin-up period. (b) Time series of sea ice
 231 area loss (perturbed minus control) in the Southern and Northern Hemispheres (blue and
 232 orange, respectively). (c) Mean annual cycle over the period of 300 years of monthly-mean sea
 233 ice area loss (perturbed minus control) in the Southern and Northern Hemispheres (blue and
 234 orange, respectively). (d) Annual cycle of monthly-mean percentage sea ice area loss in the
 235 Southern and Northern Hemispheres (blue and orange, respectively). (e) Annual cycle of
 236 monthly-mean sea ice area change (perturbation minus control) in the coupled and atmosphere-
 237 only experiments, and their difference (dashed, solid and dotted lines, respectively). (f) Annual
 238 cycle of monthly-mean turbulent heat flux change (perturbation minus control) in the coupled
 239 and atmosphere-only experiments, and their difference (dashed, solid and dotted lines,
 240 respectively). The heat flux is multiplied by the true area of each grid-box and summed over
 241 the grid-boxes where Antarctic sea ice cover is reduced.

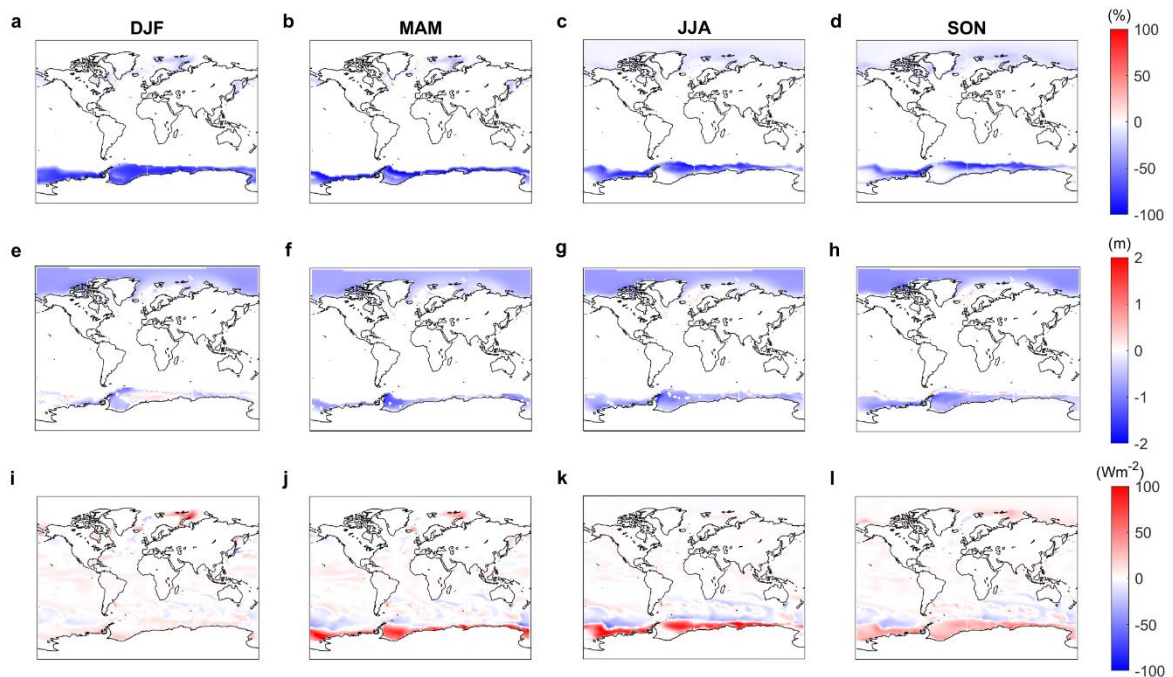
242 This seasonal cycle of ice loss, skewed towards summer, is a characteristic of albedo
243 reduction experiments, which disproportionally reduce sea ice in summer when incoming solar
244 radiation is at its maximum (Sun et al. 2020). One advantage of this approach is that energy,
245 freshwater and salt are conserved, unlike with nudging methods (Screen et al. 2018; Sun et al.
246 2019).

247 Although the albedo was only changed in the Southern Hemisphere, Arctic SIA shows 24%
248 loss in boreal summer and 5% loss in boreal winter (Figure 1d), which, although considerably
249 lesser in magnitude than in the Southern Hemisphere, demonstrates a marked reduction of
250 Arctic sea ice in response to Antarctic sea-ice loss. The Arctic sea ice response is delayed by
251 approximately twenty years compared to the imposed sea ice reduction in the Antarctic (Figure
252 1b), which suggests that the pole-to-pole response may be governed by slow oceanic processes,
253 a concept returned to later.

254 Recall, sea ice fields from the coupled model were prescribed in the atmosphere only
255 experiments. Figure 1g shows a small discrepancy between the Antarctic SIA loss in the
256 coupled and uncoupled cases, which arises because the atmospheric model (when run in
257 uncoupled mode) replaces sea ice concentrations below 30% with zeros. Further, we note
258 differences in sea ice thickness between the coupled and uncoupled cases (not shown), as in
259 the latter, sea ice thickness is derived empirically from the sea ice concentration and not
260 explicitly simulated. Despite these differences in sea ice states, the heat flux responses are very
261 similar in the coupled and uncoupled cases (Figure 1h), meaning it is appropriate to interpret
262 differences in the atmospheric response between coupled and uncoupled cases as arising due
263 to the coupling and not because of differences in forcing. In both coupled and uncoupled cases,
264 the total turbulent heat flux to the atmosphere peaks in winter at a little over 500 TW and is
265 smallest in summer at less than 100 TW. This seasonal cycle reflects both the magnitude of
266 sea-ice loss in each month and the air-sea temperature difference.

267 Sea ice concentrations are reduced all year round in the Southern Hemisphere (Figure 2a-
268 d), being of greatest magnitude near the ice edge, which migrates with the seasons. Antarctic
269 sea ice thickness is reduced everywhere within the ice pack in all seasons, except for patches
270 of thickening in summer (Figure 2e-h). In the Arctic, there are modest reductions in sea ice
271 concentration, mostly in the Barents-Kara Sea in boreal winter and spring but extending across
272 the Arctic Ocean in boreal summer and autumn (Figure 2a-d). Sea ice thickness is reduced in
273 all seasons across the Arctic and by similar magnitudes to in the Antarctic (Figure 2e-h). The

274 spatial patterns of the turbulent (sensible plus latent) heat flux responses largely mimics those
 275 of sea ice concentration, with largest increases in the ocean-to-atmosphere heat exchange in
 276 regions of ice loss, and seasonally greatest in autumn and winter (Figure 2i-l). Reductions in
 277 the turbulent heat flux are seen northward of the sea ice edge in the Southern Ocean, reflecting
 278 anomalous heat input. In the Arctic, increased heat fluxes are simulated in the colder boreal
 279 season and in regions of reduced sea ice cover, mainly the Barents-Kara Sea.

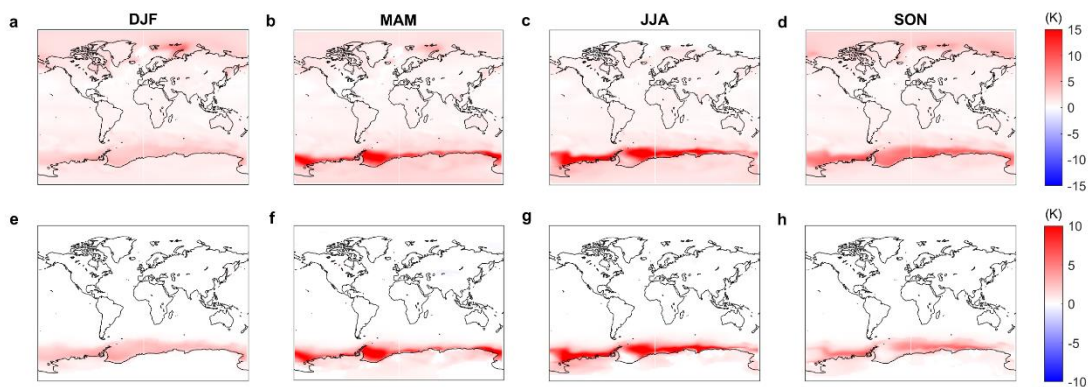


280
 281 **Figure 2.** (a-d) Sea ice concentration response, i.e., perturbed minus control, in summer,
 282 autumn, winter and spring, respectively. (e-h) As a-d but for sea ice thickness. (i-l) As a-d but
 283 for surface turbulent heat flux. The heat flux is defined positive in the upward direction, so red
 284 (blue) denotes areas where the heat flux into the ocean is higher (lower) in the perturbed
 285 experiments.

286 *b. Spatial pattern of the atmospheric response*

287 The near-surface air temperature response is global in reach in the coupled model, reaching
 288 as high as 15 K over regions of Antarctic sea-ice loss in autumn and winter (Figure 3a-d). In
 289 polar regions, there is a clear seasonal cycle, with the largest warming in autumn and winter,
 290 in each hemisphere, as expected from the heat flux response (Figure 1). An increase in
 291 temperature over the Antarctic continent is present in all seasons (Figure 3a-d), with coastal
 292 regions warming the most, by up to 5 K in winter and spring, but significant warming extending
 293 to the high-altitude plateau in all seasons. There is substantial warming of up to 4 K in the
 294 northern regions of the Southern Ocean. Over the tropics, surface warming is similar in each

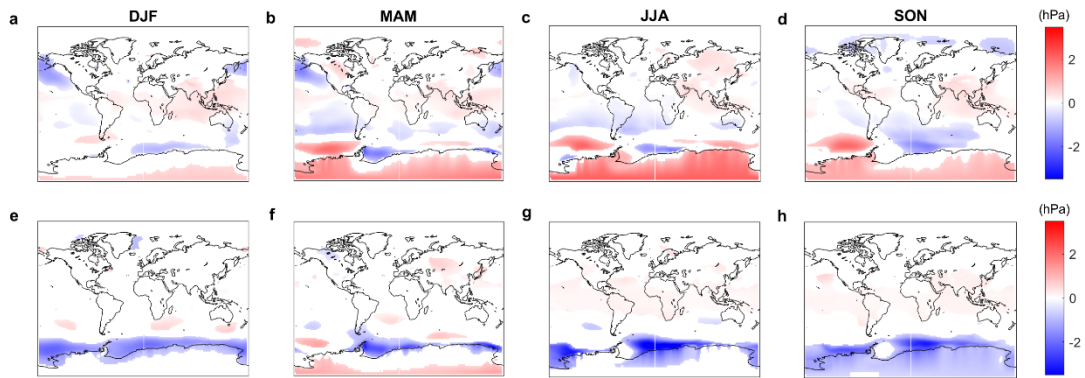
295 season, albeit of smaller magnitude than at the poles. In the high latitudes of the Northern
 296 Hemisphere, north of 50° N, there is an increase in near-surface air temperature of between 3
 297 K and 8 K, in all seasons apart from boreal summer. The largest increases in near-surface air
 298 temperature are in the Barents-Kara Sea in boreal winter, again consistent with the spatial and
 299 seasonal pattern of the heat flux response. In the atmosphere-only experiments, the warming is
 300 restricted to the regions of sea-ice loss, and the nearby Southern Ocean and coastal regions of
 301 the Antarctic continent (Figure 3e-h). Unlike in the coupled experiment, warming does not
 302 extend to the high-altitude plateau in any season or north of 50° S. A highly similar seasonal
 303 cycle is seen in the uncoupled and coupled cases, with the largest local warming in autumn and
 304 winter, but the maximum warming is ~2 K greater in the coupled compared to uncoupled
 305 experiments.



306 **Figure 3.** (a-d) Near-surface air temperature response, i.e., perturbed minus control, in austral
 307 summer, autumn, winter, and spring, respectively, in the coupled model. (e-h) As a-d but for
 308 uncoupled experiments.
 309

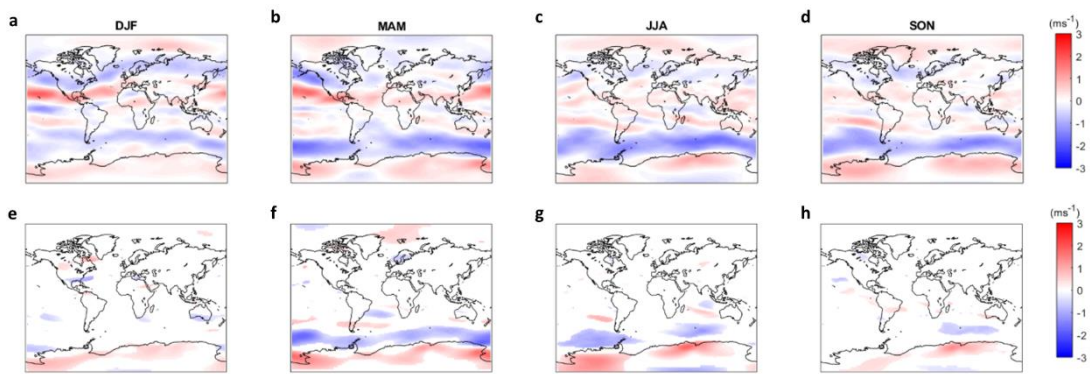
310 In the coupled experiment, the mean sea level pressure (MSLP) response (Figure 4a-d) to
 311 Antarctic sea-ice loss shows an increase over Antarctica, up to 2.2 Pa, with the largest and most
 312 significant increase in winter. This high-latitude MSLP increase maps onto the negative phase
 313 of the SAM. However, the MSLP response over the Southern Ocean is not zonally symmetric.
 314 There is a clear weakening of the Amundsen Sea Low from autumn to spring (i.e., increased
 315 MSLP), and decreased MSLP in the Weddell Sea in all seasons. North of 50° S, one notable
 316 feature is the MSLP decrease over the North Pacific, reflecting a strengthened Aleutian Low
 317 in boreal winter and spring. In the uncoupled experiments, there is a decrease in pressure of
 318 up to 3 Pa over the Southern Ocean and Antarctic continent in all seasons apart from autumn,
 319 when there is a slight increase at the highest latitudes and in the Amundsen Sea Low region
 320 (Figure 4e-h). Few regions beyond the Southern Ocean show a significant MSLP response in
 321 the uncoupled experiments, with perhaps the exception of winter, when there are patchy MSLP

322 increases over mid-latitudes. The MSLP responses in the coupled and atmosphere-only models
 323 are of opposite sign in many regions, including over Antarctica and in the Amundsen Sea Low
 324 region. Broadly speaking, the MSLP response in the uncoupled model is characterised by
 325 reduced MSLP in regions of sea-ice loss, a direct “heat low” type response, whereas the
 326 coupled model response bears closer resemblance to the negative SAM phase.



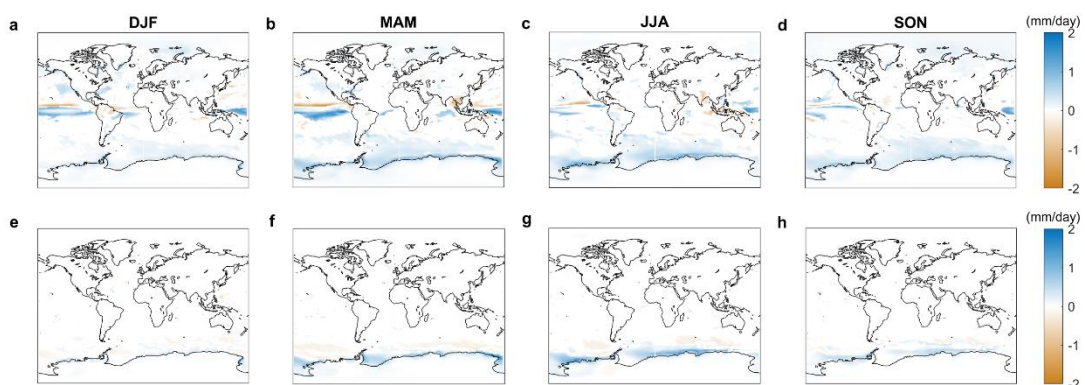
327 **Figure 4.** (a-d) Mean sea level pressure response, i.e., perturbed minus control, in austral
 328 summer, autumn, winter, and spring, respectively, in the coupled model. (e-h) As a-d but for
 329 uncoupled experiments.
 330

331 The zonal wind response at 500 hPa (U500) (Figure 5a-d) displays a decrease over the
 332 latitudes of the westerly jet in all seasons in the coupled model, suggesting a weakening of the
 333 jet, which is largest in autumn and winter. The maximum decrease, in winter, amounts to a ~10
 334 % reduction in the mean westerlies. The increase of the equatorward flank of the westerly is
 335 less significant. A similar decrease of the zonal wind in the latitudes of the westerly eddy-
 336 driven jet is seen in the uncoupled simulation, but of weaker (less than 50% of the magnitude
 337 in the coupled mode) magnitude, especially in the warmer seasons, and significant in only
 338 autumn and winter (Figure 5e-h). Thus, the weakened westerly response is seen year-round in
 339 the coupled model, but only during the colder seasons in the atmosphere-only model. The
 340 weakening is also more latitudinally confined in the atmosphere-only model response. In the
 341 Northern Hemisphere midlatitudes there is a dipole in the coupled model, suggesting an
 342 equatorward shift of the eddy-driven jet, particularly in the Pacific sector in boreal winter and
 343 spring. This feature is absent in the uncoupled experiments, which show only small, patchy
 344 regions of significant change in the Northern Hemisphere.



345 **Figure 5.** (a-d) 500 hPa zonal wind response, i.e., perturbed minus control, in austral summer,
 346 autumn, winter, and spring, respectively, in the coupled model. (e-h) As a-d but for uncoupled
 347 experiments.
 348

349 Precipitation (Figure 6a-d) significantly increases over areas of Antarctic sea-ice loss and
 350 the surrounding Southern Ocean, most strongly in autumn and winter, in both coupled and
 351 uncoupled experiments. However, the wetting signal is seen over larger swathes of the
 352 Southern Ocean in the coupled model, whereas it is locally confined to the higher latitudes in
 353 the atmosphere-only model. This greater spatial extent of the wetting signal in the coupled
 354 model, compared to that in the atmosphere-only model, is likely due to the more widespread
 355 warming (Figure 6e-h) in the coupled model, which is expected to increase moisture
 356 availability. Over the Antarctic continent in the coupled model, there is an increase of up to 0.5
 357 mm/day in the coastal regions, with higher latitudes and altitudes seeing a smaller but still
 358 significant increase in all seasons. However, there is no significant response over the continent
 359 in the uncoupled experiments. A small increase in Arctic precipitation is simulated in boreal
 360 autumn and winter, only in the coupled experiments where Arctic sea-ice is reduced.



361 **Figure 6.** (a-d) Precipitation response, i.e., perturbed minus control, in austral summer,
 362 autumn, winter, and spring, respectively, in the coupled model. (e-h) As a-d but for uncoupled
 363 experiments.
 364

365

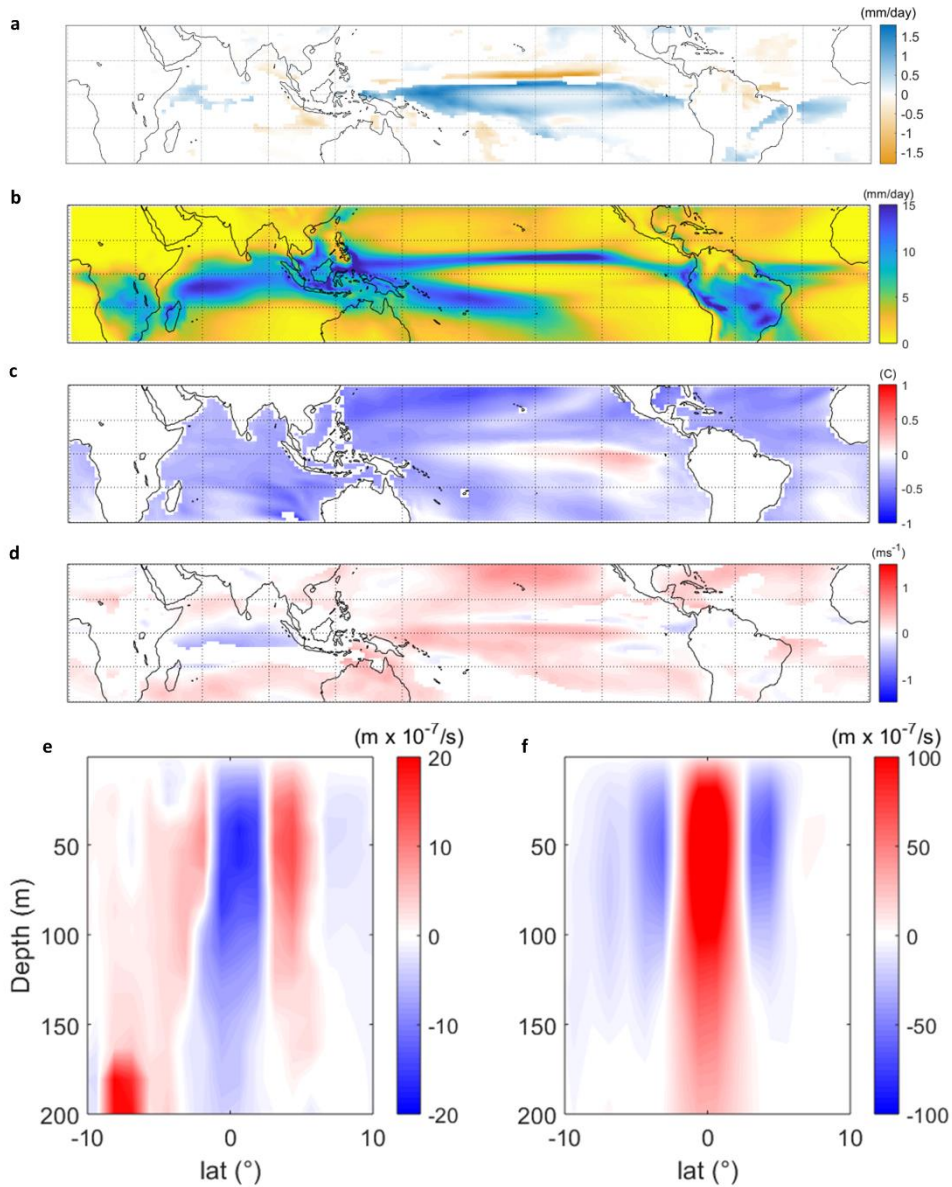
366 Precipitation changes in the tropics are also only found in the coupled model and are worthy
367 of closer examination. The annual-mean precipitation response over the tropical Pacific shows
368 a decrease in a band north of the equator, which is climatologically wetter, and an increase
369 along the equator, which is climatologically drier (Figure 7a,b). This suggests a shift of the
370 Intertropical Convergence Zone (ITCZ), analogous but of smaller magnitude to that simulated
371 in response to increased greenhouse gas concentrations (Collins et al. 2013). The spatial pattern
372 of the tropical precipitation response resembles that of SST, with increased precipitation in
373 regions of greater ocean surface warming, relative to the global mean, and reduced precipitation
374 in regions of lesser ocean surface warming, again relative to the global mean (Figure 7c; the
375 “warmer gets wetter” paradigm). Locally enhanced surface warming along the equator in the
376 Pacific Ocean is likely related to reduced upwelling of colder water from depth. Figure 7d show
377 the tropical upper ocean convergence cell in the control run. Upwelling along the equator is
378 balanced by off-equatorial downwelling. In response to Antarctic sea-ice loss, the tropical
379 convergence cell is weakened (Figure 7e), related to the weakened easterly trade winds (Figure
380 7d)

381 *c. Vertical structure of the atmospheric response*

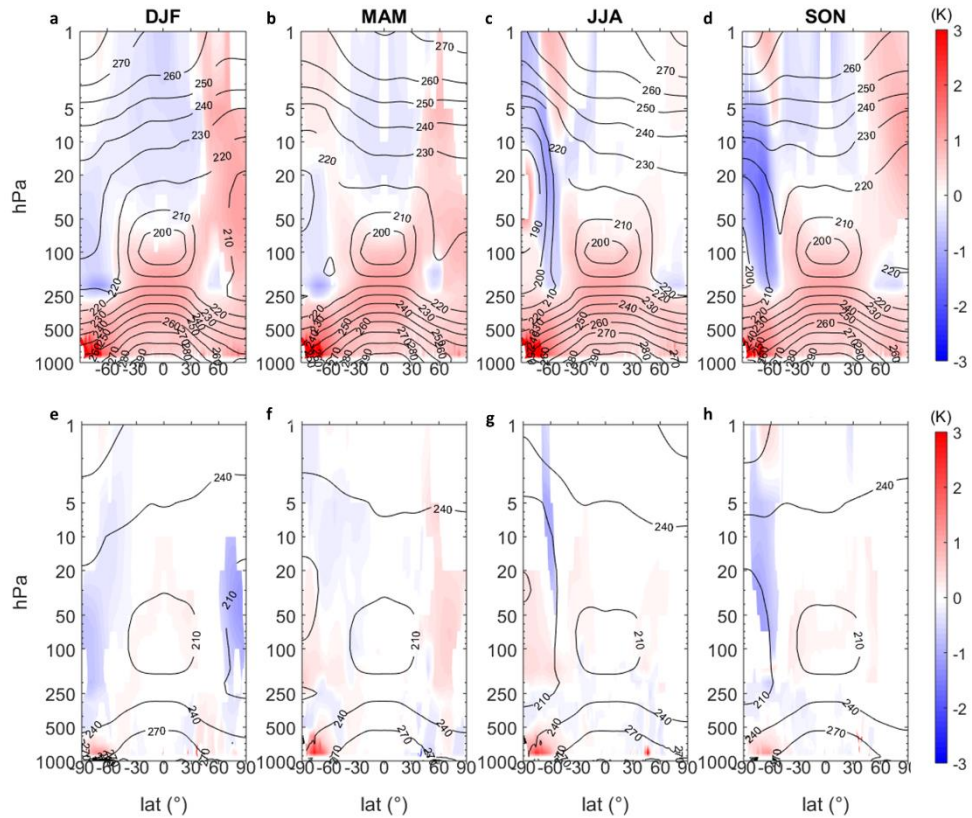
382 In the coupled model, the zonal-mean temperature response to Antarctic sea-ice loss
383 displays warming throughout the troposphere, with the biggest increase over the high southern
384 latitudes in the lower troposphere (Figure 8a-d). In the upper troposphere, there is a warming
385 at lower latitudes, akin to a classical global warming temperature signature. The stratosphere
386 cools in the Southern Hemisphere, in all seasons apart from winter. In contrast, the Northern
387 Hemisphere stratosphere warms in all seasons apart from boreal autumn. In the absence of
388 ocean coupling, the zonal-mean temperature response displays lower tropospheric warming
389 (up to 500 hPa) over Antarctica and the Southern Ocean, of greatest magnitude in autumn and
390 winter (Figure 8e-h). Although both model versions depict tropospheric warming over the
391 Antarctic and Southern Ocean, this warming is of greater magnitude and extends to higher
392 altitudes in the coupled model. Warming reaches the tropopause over the Antarctic (250 hPa)
393 in the coupled model, whereas it is confined to below 500 hPa in the atmosphere-only model.
394 The Southern Hemisphere polar stratospheric cooling is also of greater magnitude in the
395 coupled model; in fact, this region warms in autumn and winter in the uncoupled case. There
396 is a clear global tropospheric warming signature in the coupled model, which is not present in

15

397 the atmospheric-only model. The tropical upper tropospheric warming and Arctic lower
 398 tropospheric warming seen in the coupled model response are absent from the atmosphere-only
 399 model response.

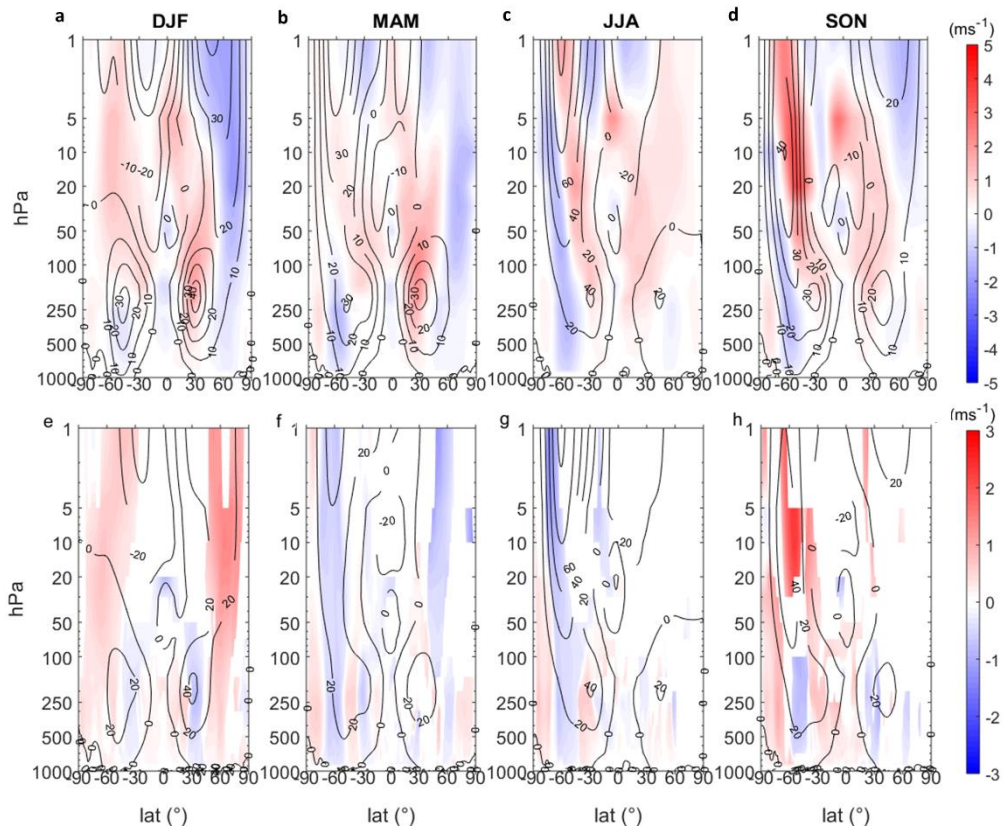


400
 401 **Figure 7.** (a) Annual-mean tropical precipitation response, i.e., perturbed minus control, in the
 402 coupled model. (b) Annual-mean tropical precipitation in the coupled control simulation. (c)
 403 As a but for sea surface temperature. Here, local changes are plotted relative to the global mean
 404 response. (d) As a but for zonal wind. (e) Zonal-mean tropical Pacific vertical ocean velocity
 405 in the top 200m in the coupled control run. (f) Zonal-mean tropical Pacific vertical ocean
 406 velocity response.



407
 408 **Figure 8.** (a-d) Zonal-mean air temperature response, i.e., perturbed minus control, in austral summer, autumn, winter, and spring, respectively, in the coupled model. (e-h) As a-d but for
 409
 410 uncoupled experiments.

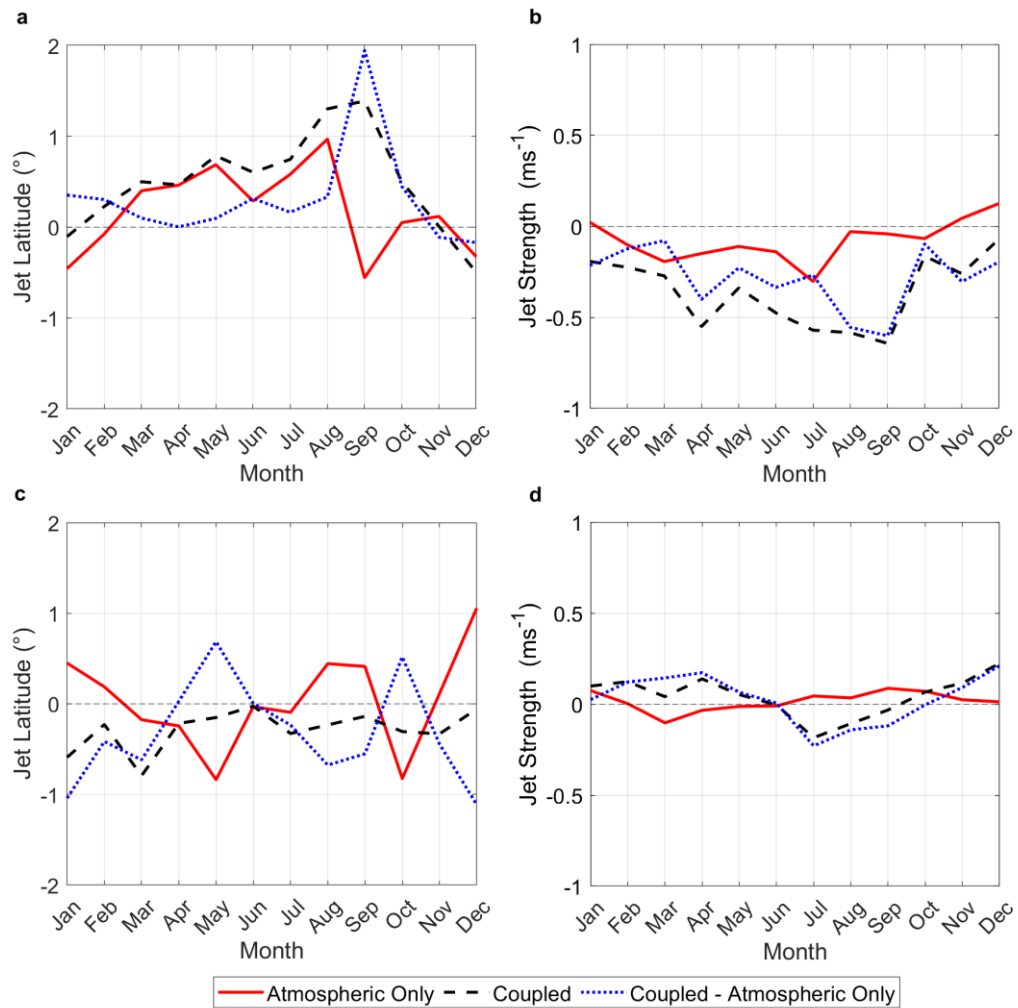
411 Turning now to the zonal-mean zonal wind response (Figure 9), the velocities decrease in
 412 the core and on the poleward flank of the Southern Hemisphere westerly jet, suggesting a
 413 weakening and slight equatorward shift of the jet. This change is seen in all seasons in both the
 414 coupled and uncoupled experiments, but is of greater magnitude in the coupled model,
 415 especially in the colder seasons. The main differences between the zonal-mean zonal wind
 416 responses in the coupled and uncoupled models are in the vicinity of the subtropical jets. In the
 417 coupled model, the westerly winds increase in the tropical upper troposphere, in both
 418 hemispheres, related to the upper tropospheric tropical warming. These features are absent in
 419 the atmosphere-only configuration. Also, in the coupled model only, velocities decrease on the
 420 poleward flank of the northern tropospheric eddy-driven jet in boreal winter and spring,
 421 suggesting an equatorward shift.



422
 423 **Figure 9.** (a-d) Zonal-mean zonal wind response, i.e., perturbed minus control, in austral
 424 summer, autumn, winter, and spring, respectively, in the coupled model. (e-h) As a-d but for
 425 uncoupled experiments.

426 *d. Responses of the jet streams*

427 The Southern Hemisphere mid-latitude eddy-driven jet shifts equatorward in most months
 428 in the coupled model, with a maximum shift of 1.39° of latitude in September (Figure 10). A
 429 similar jet shift is seen in the uncoupled models during the months March to August, with a
 430 maximum of 0.95° in August. The jet weakens throughout the entire year in the coupled model,
 431 with maximum weakening of 0.64 ms^{-1} in September, and in most months in the atmosphere-
 432 only model, with a maximum weakening in September of 0.3 ms^{-1} . The months of maximum
 433 jet weakening broadly correspond to the months with the largest equatorward shifts. Although
 434 a robust feature across the two model versions, the jet weakening is of notably greater
 435 magnitude in the coupled model than the atmosphere-only model. Ocean coupling appears to
 436 be more important for the jet strength response than the jet latitude response to Antarctic sea-
 437 ice loss.

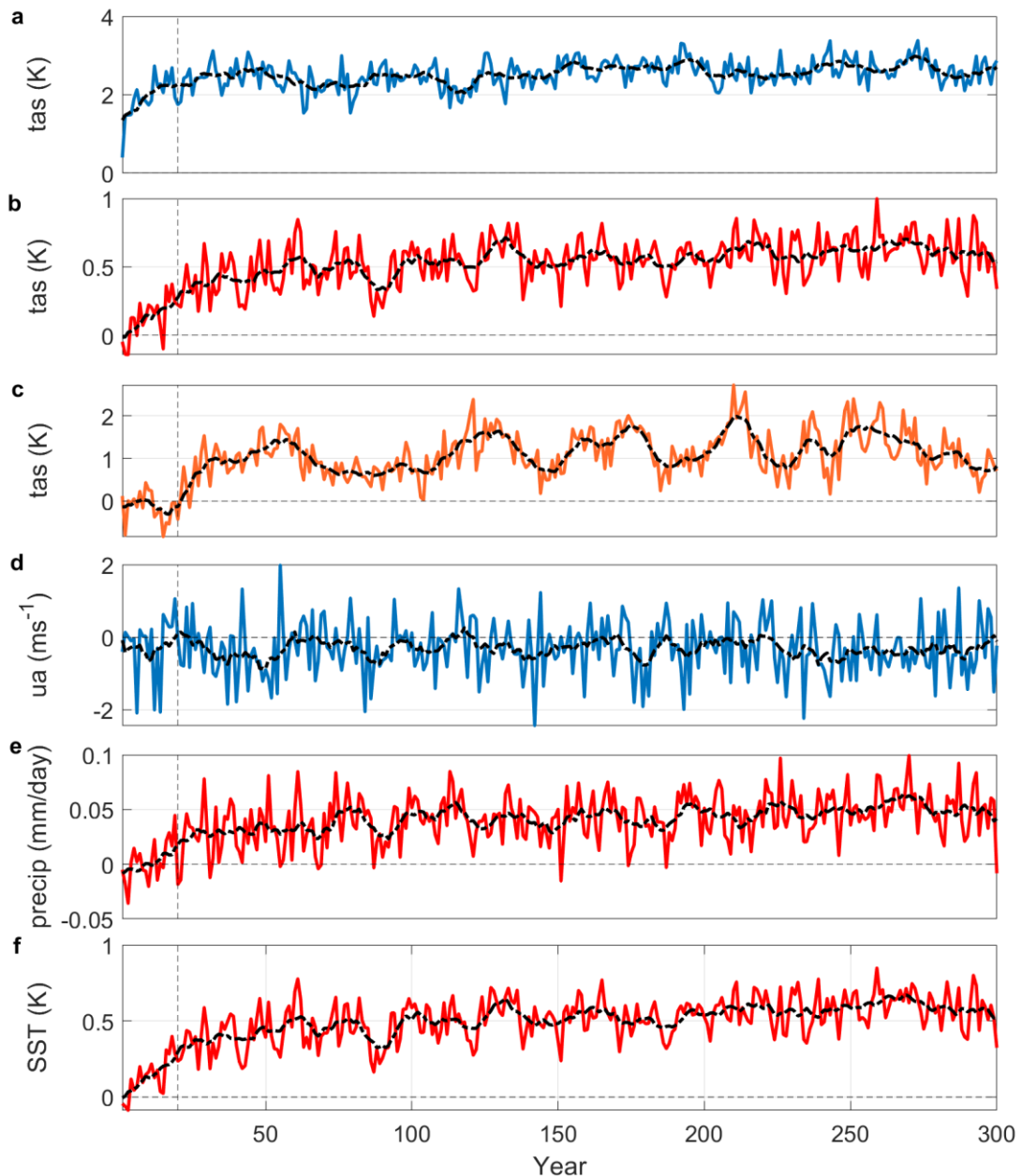


438
 439 **Figure 10.** (a) Annual cycle of the monthly-mean response of the Southern Hemisphere eddy-
 440 driven jet latitude, in the coupled and uncoupled models and their difference (black, red and
 441 blue, respectively). (b) As a but for jet strength. (c-d) As a-b but for the Northern Hemisphere
 442 eddy-driven jet.

443 In the Northern Hemisphere, the eddy-driven jet moves equatorward in all months in the
 444 coupled model, with a maximum of 0.79° in March. The jet strength increases in the boreal
 445 winter, spring, and autumn, by a maximum of 0.22 ms⁻¹ in December, but decreases in boreal
 446 summer, with a maximum of 0.18 ms⁻¹ in August. Thus, the eddy-driven jets are shifted
 447 equatorward in both hemispheres, but the jet weakening is more apparent in the Southern than
 448 Northern Hemisphere.

449 *e. Time evolution of the atmospheric response*

450 Surface warming over the Southern Hemisphere extratropics occurs rapidly following the
 451 abrupt loss of sea ice, reaching 2 K within 5 years and levelling out around 2.5 K after about
 452 30 years, with small fluctuations due to multi-decadal variability (Figure 11a). In the tropics



453
 454 **Figure 11.** (a) Time series of the annual-mean near-surface air temperature response, i.e.,
 455 perturbed minus control, averaged over Southern Hemisphere extratropics (70-40 °S). The
 456 black line denotes a 10-year running mean, the grey dashed lines denote the 20-year spin-up.
 457 (b) As a but averaged over the tropics (30 °N-30 °S). (c) As a but averaged over Northern
 458 Hemisphere extratropics (70-40 °N). (d) As a but for 500 hPa zonal wind averaged over the
 459 latitude of the westerly jet (65-35 °S). (e) As a, but for precipitation averaged over the tropics
 460 (30 N-30 °S). (f) (As a, but for sea surface temperature averaged over the tropics (30 °N-30
 461 °S).

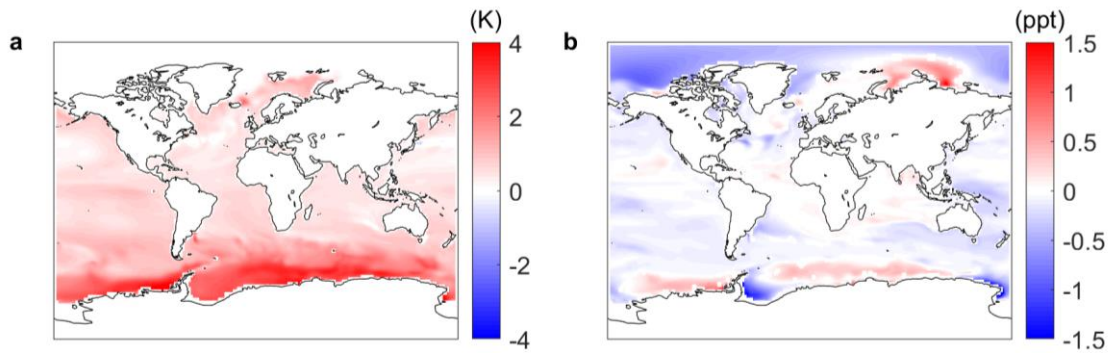
462 there is a gradual warming over the first 60 years before quasi-equilibrium is reached (Figure
 463 11b). In the Northern Hemisphere extratropics, there is little warming in the first 20 years
 464 (Figure 11c). This delay suggests a role for oceanic processes, which evolve more slowly than
 465 atmospheric processes. Recall, a similar lag was seen in the Arctic sea ice response (Figure

466 1b). Warming becomes apparent thereafter, reaching equilibrium after around 60 years (Figure
467 11c). The Southern Hemisphere tropospheric eddy-driven jet (Figure 11d) exhibits a decrease
468 in the zonal velocity from the beginning of the simulation, consistent with a fast jet weakening
469 response. There is some indication that the jet response lessens after the first seventy years,
470 which might reflect the impact of tropical warming re-establishing a stronger pole-to-equator
471 near-surface temperature difference, but not recovering back to its original state. However,
472 there is substantial internal variability which prevent firm conclusions regarding the transient
473 response. The tropical precipitation and SST responses (Figure 11e,f) follow the same
474 trajectory as tropical surface air temperature (Figure 11b), with a gradual increase over the first
475 60 years before levelling out. Thus, the tropical air temperature, SST and precipitation
476 responses appear to be governed by similar ‘slow’ processes, involving the ocean.

477 *f. Surface ocean response*

478 An increase in SST is observed globally in ice-free waters (Figure 12a). In the coastal
479 regions of the Southern Ocean, annual-mean SSTs increase by as much as 4 K, with significant
480 warming extending to the northern regions of the Southern Ocean, up to 40° S. In the tropics
481 and mid-latitudes of both hemispheres, SST increases by approximately 1 K in all ocean basins,
482 with a slightly greater increase in the tropical Pacific than the tropical Atlantic. In the Northern
483 Hemisphere, north of 50° N, there is an increase in SSTs of up to 2 K in the North Atlantic
484 region and Barents-Kara Sea.

485 A decrease in sea surface salinity in the Arctic Ocean is simulated, with the largest decrease
486 of 1.5 in the Beaufort Sea (Figure 12b). This salinity decrease is an expected result from Arctic
487 sea-ice loss (increased freshwater input and/or reduced brine rejection from ice formation), in
488 addition to the increased precipitation (Figure 6). Surface salinity is increased over the Kara
489 and Laptev Seas in the Arctic, and over the Amundsen and Weddell Seas in the Antarctic.
490 These increases in salinity may relate to changes in advection and mixing, increased
491 evaporation from larger SSTs, in addition to the seasonal melt season. Due to the ice-albedo
492 feedback, sea ice loss is heavily biased towards the summer months, which can lead to more
493 rapid ice formation in autumn and winter, leading to increased brine rejection. Otherwise,
494 decreased sea ice can lead to decreased salinity and brine rejection. The Antarctic is dominated
495 by seasonal ice cover, so the former effect dominates. Regionally, areas of greater seasonal
496 sea ice in the Antarctic show an increase in salinity, whereas regions with more multiyear ice,
497 such as the Weddell Sea, show decreased salinity.



498 **Figure 12:** (a) Annual-mean sea surface temperature response, i.e., perturbed minus control.
 499 (b) Annual-mean sea surface salinity response.
 500

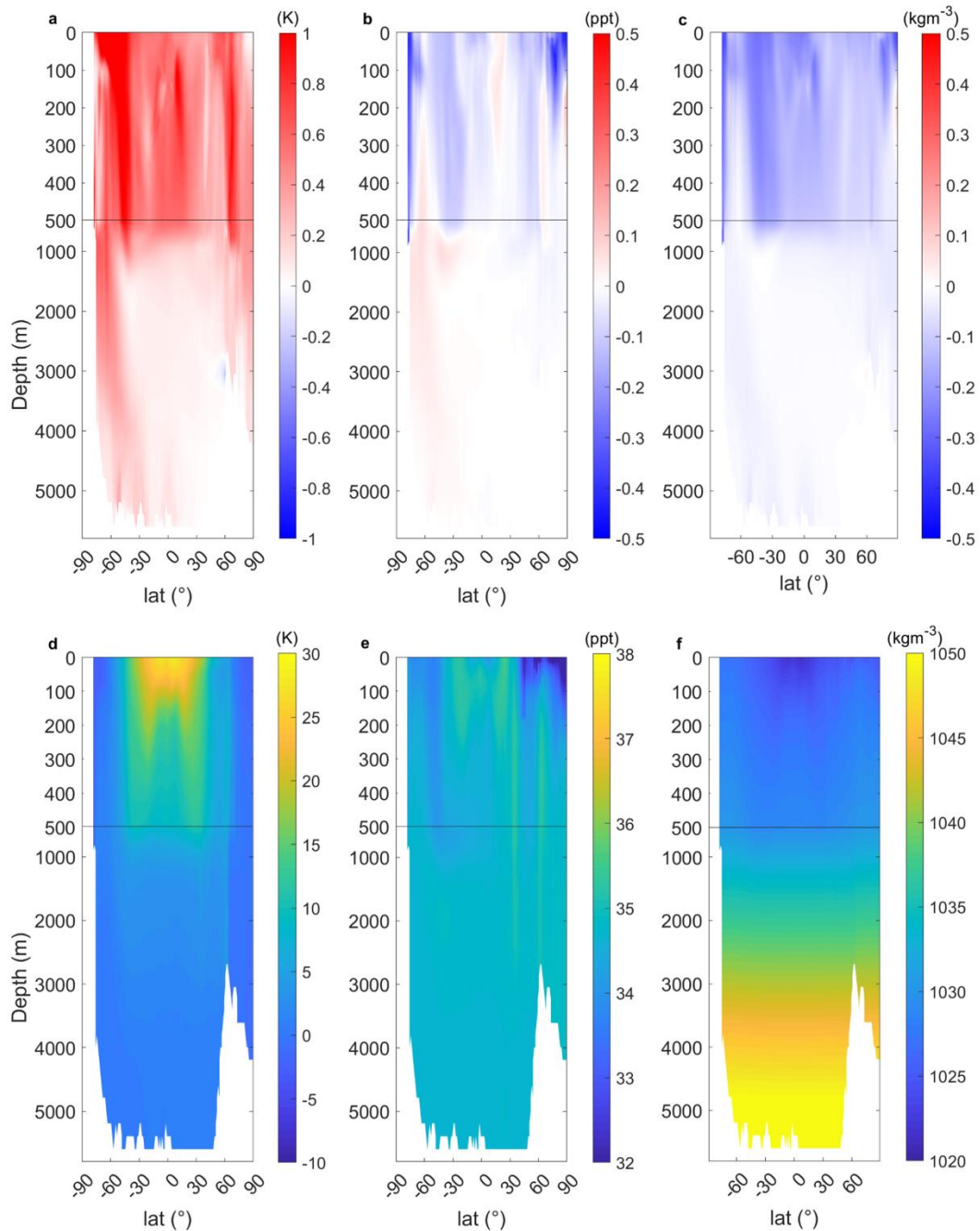
501 *g. Subsurface ocean response*

502 The zonal-mean temperature response as a function of depth shows warming at all latitudes
 503 and depths, suggesting warming of all global water masses (Figure 13a). The overall warming
 504 pattern is comparable to that seen in the RCP4.5 scenario (Collins et al., 2013), suggesting that
 505 sea-ice loss induces a ‘mini global warming’ signature in the ocean, analogous to that in the
 506 atmosphere. Water in the top 1000 m shows the largest increases, with the greatest warming
 507 south of 30° S in all basins, followed by north of 60° N, and then hotspots around the equator.
 508 Warming is not limited to the mixed layer, highlighting the role of ocean circulation and mixing
 509 in the global response to Antarctic sea-ice loss. In the Southern Ocean, there is marked warming
 510 at depth. Antarctic Bottom Water (AABW) is a crucial water mass for the Meridional
 511 Overturning Circulation and its temperature increases by up to 1 K (and becomes less dense),
 512 potentially reducing downwelling in the region.

513 Salinity decreases by ~ 0.9 in surface and intermediate waters at most latitudes and
 514 increases by ~ 0.2 in the deep-water masses of the Southern Ocean (Figure 13b). Salinity can
 515 be controlled by a variety of factors. The simulated increase in precipitation (Figure 6) acts to
 516 reduce salinity at the surface, and ice melt and reduced ice growth (brine rejection) also
 517 contribute to freshening. Salinity increases at depth are more likely due to changes in advection
 518 by both the meridional and vertical transports.

519 A combination of the freshening and warming leads to a reduction in density in surface waters
 520 globally, and in deep waters generated near the Antarctic coast (Figure 13c). The increase in
 521 the temperature of AABW is partially counteracted by the increase in salinity, but not enough
 522 to offset it, so its density is still reduced. Surface waters show a maximum decrease in density

523 of $\sim 0.5 \text{ kgm}^{-3}$, with AABW and North Atlantic Deep Water (NADW) decreasing by ~ 0.2
 524 kgm^{-3} . Having less dense water at the surface may reduce upwelling, acting as a stable lid in
 525 polar regions.



526 **Figure 13.** (a) Zonal- and annual-mean potential seawater temperature response, i.e., perturbed
 527 minus control. Note that a discontinuous depth axis has been used to highlight the features in
 528 the top 500m. (b) As a but for salinity. (c) As a but for density. (d) Zonal- and annual-mean
 529 temperature in the coupled control experiment. (e) As d but for salinity. (f) As d but for density.

531

532 Vertical temperature-salinity (T-S) profiles are presented in Figure 14 to assess changes to
533 the water column and in characteristic water masses. T-S profiles show how the density of the
534 water changes as a function of potential temperature and salinity. Where density increases with
535 depth, the water column is considered stable, which restricts vertical mixing. Conversely,
536 decreasing density with depth implies an unstable water column, conducive to vertical mixing.
537 Key water masses can be recognized on a T-S diagram by their specific tracer properties.
538 Typically, the bend point identifies the core of the water mass and the lines between the bend
539 points represent mixing between adjacent water masses. Due to the non-linear relationship
540 between temperature and density, temperature change is the dominant driver of density change
541 in warmer waters (visually, this appears in the T-S plot as more tilted isopycnals), whereas
542 salinity change is the dominant driver of density change in colder waters (seen as more
543 vertically aligned isopycnals).

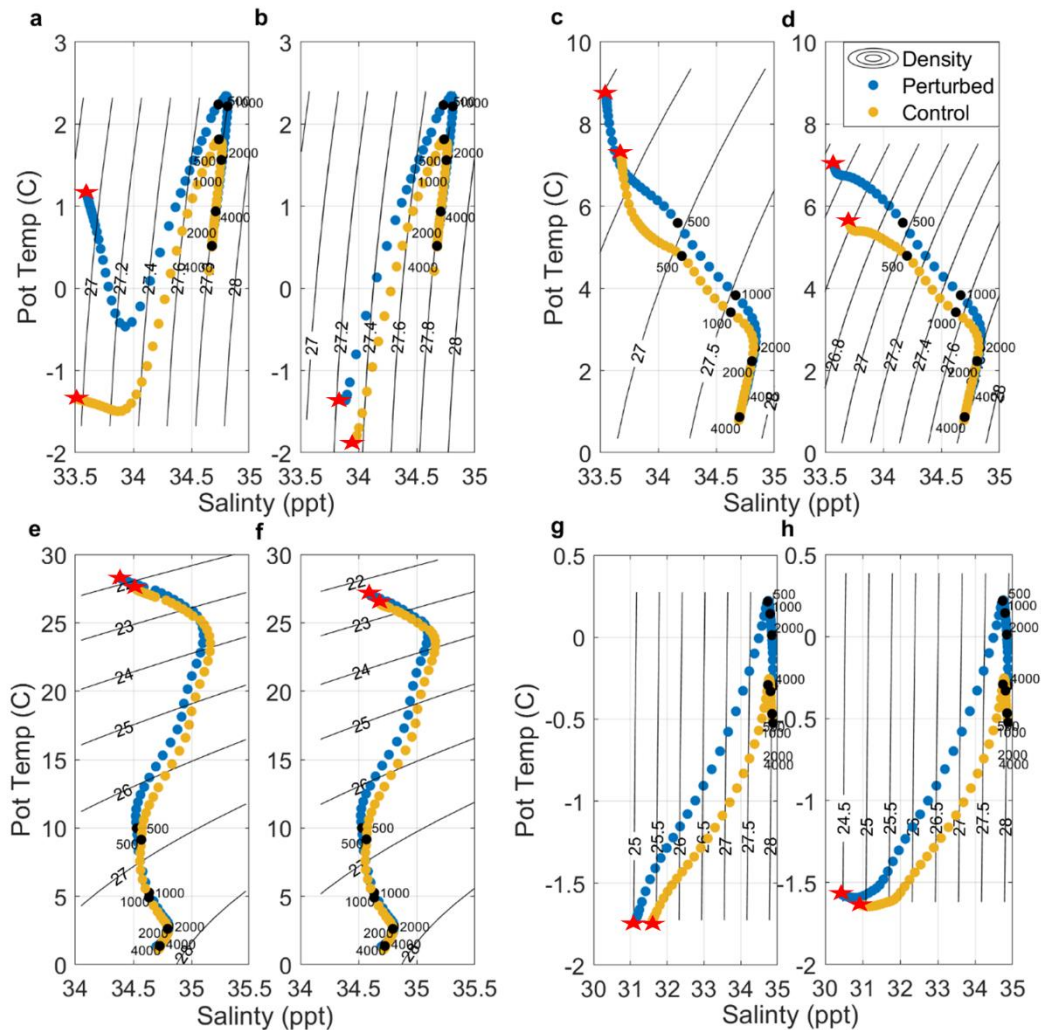
544 In the Southern Ocean at 70 °S, colder surface waters overlie warmer waters at depth. In
545 the warm season, surface waters above the seasonal thermocline are warmed and freshened by
546 sea-ice loss, leading to a weakened density gradient in the upper layers and thus, a reduced
547 mixed layer depth (Figure 14a). Below the seasonal thermocline in warm season, and
548 throughout the water column in the cold season, water masses remain approximately the same
549 density, despite warming (i.e., the profiles are shifted along isopycnals in Figure 14a,b). Recall
550 that at this latitude, density is controlled by salinity more than temperature (i.e., the isopycnals
551 are nearly vertical).

552 In the Southern Ocean at 50 °S, the entire water column warms in response to sea-ice loss,
553 year-round, with the biggest increase of 1.5 K at the surface, above the seasonal thermocline
554 (Figure 14c,d). Salinity is reduced in the surface and intermediate waters, again in all seasons.
555 Sea-ice loss results in less dense surface waters in all seasons (warmer and fresher; recall that
556 at this latitude, temperature change dominates over salinity change in the density response),
557 meaning a more stable water column and increased stratification in the upper ocean. Although
558 a year-round increase in both temperature and salinity is found in the Deep Waters and AABW,
559 the density of these waters remains largely the same, and hence the structure of the water
560 column at these depths is unchanged. Therefore, at 50 ° S the greatest changes to density occur
561 toward the top of the water column.

562 In the tropics, the water column is warmer than at high southern latitudes and thus, changes
563 in temperature are more important than changes in salinity for determining the density response

564 (note the near-horizontal isopycnals in Figure 14e, f). At the equator, there are smaller
565 differences in salinity or temperature in response to sea-ice loss than in the Southern Ocean.
566 The maximum response in the water column is at the surface, where there is warming of ~1 K
567 and a slight freshening of 0.1. At depth, there is a small decrease in salinity and warming of
568 intermediate waters, but minimal change in Deep Waters. Overall, the profiles show a slight
569 decrease in density in response to sea-ice loss from intermediate levels to the surface.

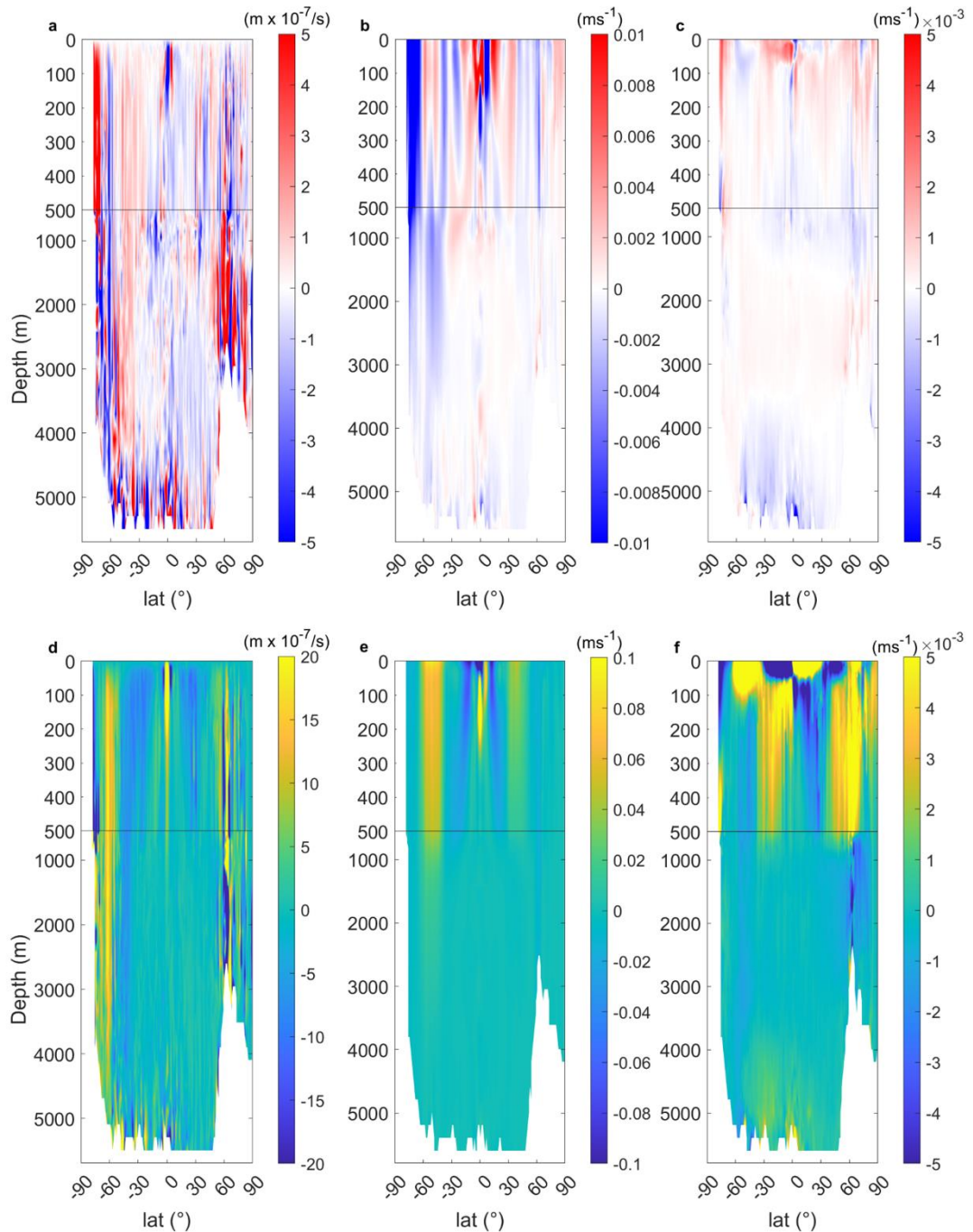
570 In the Arctic Ocean at 85 °N, surface and intermediate waters warm by 0.5 K (Figure
571 14g,h). At greater depth, the response is dominated by changes in salinity (i.e., the curves are
572 shifted horizontally), specifically freshening, likely in response to induced Arctic sea-ice loss.
573 In the Arctic Ocean, density changes are very strongly determined by salinity changes (i.e.,
574 near vertical isopycnals) and hence, salinity determines stratification. The vertical density
575 structure of the water column is largely unchanged, but density is reduced at in the upper 500m,
576 which increases the stability of the water column and reduces vertical mixing.



577
 578 **Figure 14.** (a) Zonal-mean temperature-salinity profiles at 70 °S for the warm season. Orange
 579 dots show the control experiment and blue dots the perturbed experiment. Depth and water
 580 density increase from left to right across the figure, red stars denote top of water column. Black
 581 curves denote isopycnals, i.e., lines of constant density and the black dots denote depth. (b) As
 582 a but for the cold season. (c, d) As a, b but at 50 °S. (e, f) As a, b but at the equator. (g, h) As
 583 a, b but at 85 °N.

584 *h. Ocean circulation changes*

585 The zonal-mean zonal velocity in the Southern Ocean is dominated by the Antarctic
 586 Circumpolar Current (ACC) and the Antarctic coastal current (Figure 15b), both driven by the
 587 wind. In the latitudes of the ACC (~ 40-60 °S), zonal velocity in the upper ocean increases on
 588 the southern flank and decreases on the northern flank. With depth, a more consistent decrease
 589 in zonal velocity is seen within the ACC. In the tropics, there is a reduction in the equatorial
 590 currents.



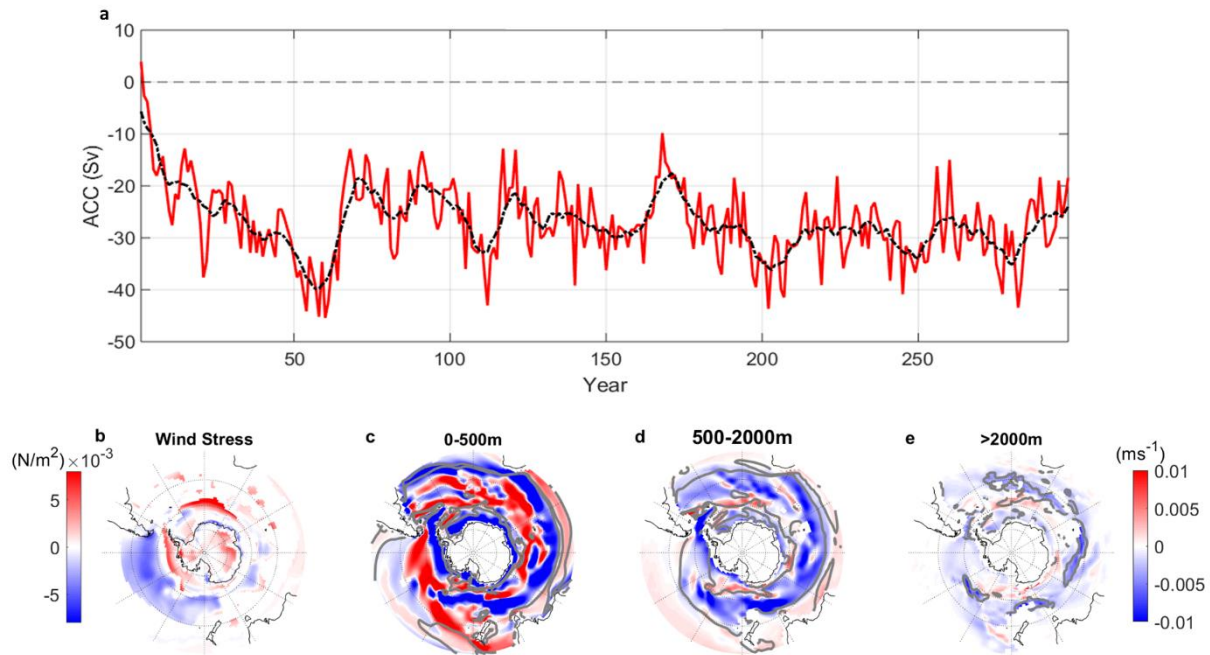
591 **Figure 15.** (a) Zonal- and annual-mean vertical velocity response, i.e., perturbed minus control.
 592 Note that a discontinuous depth axis has been used to highlight the features in the top 500m.
 593 (b) As a but for zonal velocity response. (c) As a but for meridional velocity response. (d)
 594 Zonal- and annual-mean vertical velocity in the coupled control experiment. (e) As d but for
 595 zonal velocity. (f) As d but for meridional velocity.

597 Changes in the zonal-mean meridional velocity are small in comparison to the zonal
 598 velocity response (Figure 15d). Within the ACC, there is a decrease in northward velocity. At
 599 depth (~4000-5000m), the mean northward velocity of Antarctic Bottom Water (AABW) is
 600 decreased at latitudes 30 °N – 60 °S. The surface water of the tropics shows a reduced

601 southward velocity in the Southern Hemisphere (northward response in region of mean
602 southward flow, c.f. Figure 15b,d), and reduced northward velocity in the Northern Hemisphere
603 (southward response in region of mean northward flow, c.f. Figure 15c,f), related to the reduced
604 equatorial upwelling and weakened overturning of the tropical convergence cell (Figure 7). At
605 2000-4000m depth, the mean southward transport of NADW is slightly reduced in latitudes
606 40-80 °N (Figure 15 f).

607 The zonal-mean vertical velocity provides insight into changes in mixing resulting from
608 density and wind driven processes. Throughout the Southern Ocean, downwelling of bottom
609 waters at the very high latitudes off the coastal shelf is reduced (i.e., there is generally an
610 upward velocity response in regions of climatological downwelling, c.f. Figure 15a,d). Also,
611 upwelling of deep waters in latitudes 60-70 °S is reduced (i.e., generally a downward velocity
612 response in regions of climatological upwelling). At lower latitudes of the Southern Ocean,
613 climatological downwelling is reduced by sea-ice loss. Equatorial upwelling of cold water in
614 the tropics is also weakened, as discussed earlier.

615 A marked decrease in the ACC volume transport of 25-40 Sv is simulated (Figure 16a), but
616 with little seasonal variation (not shown). This is a reduction of 18% compared to the mean
617 ACC transport in the control run (~ 150 Sv). Annual-mean ACC volume transport declines
618 steadily from the beginning of the simulation for about seventy years, and thereafter, fluctuates
619 around a lower mean (~27 Sv), not recovering back to its original state. The decreased ACC
620 transport appears to partially be in response to the weakened overlying zonal wind stress
621 (Figure 16b). Annual-mean zonal wind stress is broadly reduced along the path of the ACC,
622 especially over the Pacific and Indian sectors. Whilst the depth integrated ACC transport
623 through Drake Passage decreases, there is both spatial and vertical variability in the zonal
624 velocity response to sea-ice loss. In the top 500 m, there are filaments of increased and
625 decreased zonal flow within the latitudes of the ACC (Figure 16c). At 500-2000 m depth, a
626 clearer pattern of decreased zonal velocity emerges over the latitudes of the ACC (Figure 16d).
627 A greater depth, below 2000 m, the zonal velocity is broadly decreased, but with lesser
628 magnitude than at intermediate depths (Figure 16e). However, the mean ACC transport at depth
629 is also weaker (Figure 15b).



630
 631 **Figure 16.** (a) Time-series of annual-mean ACC transport response, i.e., perturbed minus
 632 control. The black curve denotes a 10-year running mean. (b) Annual-mean wind stress
 633 response. (c) Annual-mean zonal velocity response averaged over the top 500 m. (d) As c but
 634 averaged between 500-2000m. (e) As c but averaged below 2000m.

635

636 4. Discussion

637 The results presented suggest an important role for ocean coupling, both in amplifying local
 638 changes and in generating far-field responses. The local warming and wetting responses were
 639 approximately twice as large in the coupled model as the uncoupled model. This is comparable
 640 to Deser et al. (2016), which reported that ocean coupling amplified the warming response to
 641 Arctic sea-ice loss by approximately 50%. Warming in the coupled model reached the
 642 Antarctic continental interior, but did not in the atmosphere-only model, consistent with
 643 England et al. (2018; 2020a; 2020b) that used different climate models and sea ice loss
 644 methods. This may be for similar reasons to those proposed in the Arctic (e.g., Blackport &
 645 Kushner, 2017), whereby the coupling allows for the surrounding oceans to warm and then
 646 warm anomalies are transported along isentropic surfaces (Laliberté and Kushner 2013) from
 647 the mid-latitude ocean surface to the high-latitude mid-troposphere. In addition to the ‘fast’
 648 and largely local responses, the coupled model experiments revealed additional ‘slow’ and
 649 global responses. The coupled model displays a clear “mini-global warming” signature, with
 650 warming maxima in the high-latitude lower troposphere and tropical upper-troposphere. The

651 tropical warming, thought to be primarily driven through warmer tropical SSTs and enhanced
652 convection through a weakening of the easterly trade winds, is absent in the atmosphere-only
653 model, strongly suggesting that ocean coupling is vital in communicating Antarctic changes to
654 the rest of the globe. This result is also consistent with England et al. (2020a; 2020b), and
655 echoes the response to Arctic sea-ice loss (e.g Blackport & Kushner, 2016; Deser et al., 2016;
656 Deser et al., 2015; Oudar et al., 2017), which has also been shown to be locally confined in
657 atmospheric-only models but global in reach in coupled models. Globally, the patterns of ocean
658 warming and salinity change with latitude and depth were alike that in response to increased
659 CO₂ (e.g., Collins et al., 2013), but lesser in magnitude. Thus, it is also appropriate to think of
660 the oceanic response to Antarctic sea-ice loss as a ‘mini global warming’ response, as well as
661 the atmospheric response.

662 Another distinct aspect of the response to Antarctic sea-ice loss, seen in coupled but not in
663 uncoupled experiments, is warming in the Arctic and associated Arctic sea-ice loss, similar to
664 that reported in England et al. (2020b). It is hypothesised that the mechanism for this pole-to-
665 pole connection involves the ocean, as there is an approximate 20-year lag between the initial
666 Antarctic sea-ice loss and the resulting Arctic sea ice response. One possible mechanism is
667 tropical to northern extratropical teleconnections triggered by changes in tropical precipitation
668 (i.e., convection). Antarctic sea-ice loss causes a deepening of the Aleutian Low, observed in
669 the surface pressure response, which may be triggered by a Rossby wave train from the tropical
670 Pacific (e.g. England et al., 2020b; McCrystall et al., 2020; Yuan et al., 2018). Seasonally, the
671 deepening of the Aleutian Low is greatest in boreal winter, when tropical to extratropical
672 teleconnections are known to be most active. The seasonality of this response is also in
673 agreement with England et al. (2020b). Similarly, at high southern latitudes the more
674 pronounced weakening of the Amundsen Sea Low in austral winter (and transitional seasons)
675 is consistent with a Rossby wave train response to the tropical Pacific (Turner, 2004).

676 A significant shift equatorward of the mid-latitude tropospheric eddy-driven jet, leading to
677 a more negative SAM index and most prominent in austral autumn and winter, was simulated
678 in both the coupled and atmospheric-only experiments. Jet strength was weakened during most
679 of the year, but with lesser magnitude in the atmosphere-only model compared to the coupled
680 model. Jet strength is highly dependent on the meridional temperature gradient (and
681 baroclinity), which is decreased more in the coupled model than in the atmosphere-only model.
682 By contrast, the jet shift seems less dependent on the magnitude of high latitude warming. Jet

683 shifts may be more dependent on the initial position of the jet (Bracegirdle et al. 2018; Simpson
684 et al. 2021). Although the jet response is qualitatively similar to that seen in past studies using
685 atmosphere-only models (Bader et al., 2013; England et al., 2018; Kidston et al., 2011;
686 Menéndez et al., 1999; Raphael et al., 2011; Smith et al., 2017), the lack of ocean coupling in
687 prior studies means it may have been underestimated. The jet response to Antarctic sea-ice loss
688 acts to slightly offset the strengthening and poleward shift of the jet in response to increased
689 CO₂ (e.g., Barnes and Polvani 2013), analogous to the “tug-of-war” on the Northern
690 Hemisphere jet between Arctic sea-ice loss and increased CO₂ (e.g., Deser et al., 2016).

691 Oceanic responses to Antarctic sea-ice loss included changes to density, temperature,
692 stratification, and mixing, in the Southern Ocean; a reduction in the ACC transport at mid-
693 depths; a weakening of the tropical shallow convergence cell; and freshening of the Arctic
694 Ocean due to Arctic sea-ice loss. The zonally averaged temperature response with depth is
695 similar to that of the atmosphere, and is comparable to a ‘mini global warming’ response
696 (Collins et al., 2013). ACC transport was reduced by ~20% in the perturbed simulation in
697 comparison to the control, consistent with reduced surface wind stress due to a weakening of
698 the tropospheric eddy-driven jet. The reverse - a small increase in ACC transport in response
699 to increased sea ice and a strengthened westerly jet - was found by Downes et al. (2011).
700 However, the effect of changes in westerly jet strength on the ACC is still a matter of some
701 debate (e.g., Böning et al., 2008; Farneti & Delworth, 2010; Farneti et al., 2010; Hallberg and
702 Gnanadesikan, 2006). Shi et al. (2021) found an increase in ACC transport in response to
703 Southern Ocean warming, noting that the wind stress had a secondary role to temperature. That
704 our simulations show a reduction in ACC transport despite Southern Ocean warming, further
705 points to a key role for reduced wind stress and/or increased salinity at the shelf. A possible
706 limitation of the low resolution HadGEM3-GC3.1-LL model is that it parametrizes the effects
707 of mesoscale eddies. It is plausible that a different ACC response to sea-ice loss would have
708 been obtained if the model resolved eddies (e.g., Munday et al., 2013), albeit the response is
709 broadly consistent (but opposite in sign) to Downes et al. (2010), that used an eddy-permitting
710 model.

711

712 **5. Summary and Conclusions**

713 The climate impacts of Antarctic sea-ice loss have not been researched to the same extent
714 as the impacts of Arctic sea-ice loss. This study was one of the first to assess the coupled
715 climate response to Antarctic sea-ice loss, which can be summarised as follows. Abrupt
716 Antarctic sea-ice loss immediately caused an enhanced heat flux from ocean to atmosphere,
717 triggering localised tropospheric warming and wetting. Strong warming and freshening of
718 surface waters in the Southern Ocean led to a more stratified and stable water column. The
719 equator-to-pole temperature gradient was reduced, and thus, the tropospheric eddy-driven jet
720 was weakened, projecting onto the negative SAM phase. Weakened surface wind stress
721 contributed to a 20% reduction in the ACC transport, and reduced the northward Ekman
722 transport of cold water, further warming the upper Southern Ocean. Warmed Southern Ocean
723 SSTs allowed the atmosphere warming to spread from the Southern midlatitudes to the
724 Antarctic plateau by advection; supported by the absence of such continental warming in
725 uncoupled experiments. Over several decades, ocean surface warming reached the tropics.
726 Here, reduced easterly equatorial winds led to a weakened upper ocean tropical convergence
727 cell, and reduced upwelling of cold water, further enhancing the surface warming. Warmer
728 tropical SSTs may have enhanced convection and drove upper tropospheric warming,
729 triggering anomalous teleconnections into the extratropics, for example, strengthening the
730 Aleutian Low. Further supporting a key role for ocean coupling, analogous uncoupled
731 experiments yielded an atmospheric response much more locally confined compared to that in
732 the coupled model. Twenty to fifty years later in the coupled runs, after the abrupt loss of
733 Antarctic sea-ice, warming reached the Arctic, triggering Northern Hemisphere sea-ice loss
734 and thereby, near-surface warming and freshening of the Arctic Ocean. Both the atmospheric
735 and oceanic responses are much like those projected for scenarios of increased greenhouse
736 gases, but with lesser magnitude.

737

738 *Acknowledgments.*

739 We thank Katy Sheen and Julie Jones for their valuable discussion and comments on results
740 included in this paper. We also thank Leon Hermanson and Rosie Eade for contribution to the
741 ensemble models. PiControl Met Office HadGEM3-GC31-LL data was obtained from the
742 Earth System Grid Federation and Centre for Environmental Data Analysis, submitted as part
743 of the Climate Model Intercomparison Project Phase 6. This study was supported by the
744 “Robust Spatial Projections of Real-World Climate Change” (NERC, Research grant

745 NE/N018486/1) and the University of Exeter. EB and the development of the HadGEM3-GC31
746 climate model were supported by the Met Office Hadley Centre Climate Programme funded
747 by BEIS.

748 *Data Availability Statement.*

749 The numerical model simulations upon which this study arises based are too large to
750 archive in full. Requests for selected output should be sent to the corresponding author. The
751 coupled control simulation can be found via the Earth Earth System Grid Federation and Centre
752 for Environmental Data Analysis submitted as part of the Climate Model Intercomparison
753 Project Phase 6.

754 REFERENCES

755 Andrews, M. B., and Coauthors, 2020: Historical Simulations With HadGEM3-GC3.1 for
756 CMIP6. *J. Adv. Model. Earth Syst.*, 12, 1–34, <https://doi.org/10.1029/2019MS001995>

757 Ayres, H. C., and J. A. Screen, 2019: Multimodel Analysis of the Atmospheric Response to
758 Antarctic Sea Ice Loss at Quadrupled CO₂. *Geophys. Res. Lett.*, 46, 9861–9869,
759 <https://doi.org/10.1029/2019GL083653>.

760 Bader, J., M. Flügge, N. G. Kvamstø, M. D. S. Mesquita, and A. Voigt, 2013: Atmospheric
761 winter response to a projected future Antarctic sea-ice reduction: A dynamical analysis.
762 *Clim. Dyn.*, 40, 2707–2718, <https://doi.org/10.1007/s00382-012-1507-9>.

763 Barnes, E. A., and L. M. Polvani, 2013: Response of the Midlatitude Jets, and of Their
764 Variability, to Increased Greenhouse Gases in the CMIP5 Models. *J. Clim.*, 26, 7117–
765 7135, <https://doi.org/https://doi.org/10.1175/JCLI-D-12-00536.1>.

766 Bintanja, R., G. J. Van Oldenborgh, S. S. Drijfhout, B. Wouters, and C. A. Katsman, 2013:
767 Important role for ocean warming and increased ice-shelf melt in Antarctic sea-ice
768 expansion. *Nat. Geosci.*, 6, 376–379, <https://doi.org/10.1038/ngeo1767>.

769 Blackport, R., and P. J. Kushner, 2016: The transient and equilibrium climate response to
770 rapid summertime sea ice loss in CCSM4. *J. Clim.*, 29, 401–417,
771 <https://doi.org/10.1175/JCLI-D-15-0284.1>.

772 Blackport, R., and P. J. Kushner, 2017: Isolating the atmospheric circulation response to
773 arctic sea ice loss in the coupled climate system. *J. Clim.*, 30, 2163–2185,
774 <https://doi.org/10.1175/JCLI-D-16-0257.1>.

775 Blackport, R., & Screen, J. A. (2020). Insignificant effect of arctic amplification on the
776 amplitude of midlatitude atmospheric waves. *Science Advances*, 6(8), 277–286.eaay2880.
777 <https://doi.org/10.1126/sciadv.aay2880>

778 Böning, C. W., A. Dispert, M. Visbeck, S. R. Rintoul, and F. U. Schwarzkopf, 2008: The
779 response of the antarctic circumpolar current to recent climate change. *Nat. Geosci.*, 1,
780 864–869, <https://doi.org/10.1038/ngeo362>.

781 Bracegirdle, T. J., P. Hyder, and C. R. Holmes, 2018: CMIP5 Diversity in Southern Westerly
782 Jet Projections Related to Historical Sea Ice Area: Strong Link to Strengthening and
783 Weak Link to Shift. *J. Clim.*, 31, 195–211, <https://doi.org/10.1175/JCLI-D-17-0320.1>.

784 Briegleb, B. P., and B. Light, 2007: A Delta-Eddington Multiple Scattering Parameterization
785 for Solar Radiation in the Sea Ice Component of the Community Climate System Model.
786 100 pp.

787 Ceppi, P., G. Zappa, T. G. Shepherd, and J. M. Gregory, 2017: Fast and slow components of
788 the extratropical atmospheric circulation response to CO₂ forcing. *J. Clim.*, 31, 1091–
789 1105, <https://doi.org/10.1175/JCLI-D-17-0323.1>.

790 Cohen, J., and Coauthors, 2014: Recent Arctic amplification and extreme mid-latitude
791 weather. *Nat. Geosci.*, 7, 627–637, <https://doi.org/10.1038/ngeo2234>.

792 Collins, M., and Coauthors, 2013: Long-term Climate Change: Projections, Commitments
793 and Irreversibility. *Clim. Chang. 2013 Phys. Sci. Basis. Contrib. Work. Gr. I to Fifth*
794 *Assess. Rep. Intergov. Panel Clim. Chang.*, 1029–1136,
795 <https://doi.org/10.1017/CBO9781107415324.024>.

796 Deser, C., R. A. Tomas, and L. Sun, 2015: The role of ocean-atmosphere coupling in the
797 zonal-mean atmospheric response to Arctic sea ice loss. *J. Clim.*, 28, 2168–2186,
798 <https://doi.org/10.1175/JCLI-D-14-00325.1>.

799 Deser, C., L. Sun, R. A. Tomas, and J. Screen, 2016: Does ocean coupling matter for the
800 northern extratropical response to projected Arctic sea ice loss? *Geophys. Res. Lett.*, 43,
801 2149–2157, <https://doi.org/10.1002/2016GL067792>.

802 Downes, S. M., N. L. Bindoff, and S. R. Rintoul, 2010: Changes in the subduction of
803 Southern Ocean water masses at the end of the twenty-first century in eight IPCC models.
804 *J. Clim.*, 23, 6526–6541, <https://doi.org/10.1175/2010JCLI3620.1>.

805 Downes, S. M., A. S. Budnick, J. L. Sarmiento, and R. Farneti, 2011: Impacts of wind stress
806 on the Antarctic Circumpolar Current fronts and associated subduction. *Geophys. Res.*
807 *Letts.*, 38, 3–8, <https://doi.org/10.1029/2011GL047668>.

808 Eayrs, C., X. Li, M. N. Raphael, and D. M. Holland, 2021: Rapid decline in Antarctic sea ice
809 in recent years hints at future change. *Nat. Geosci.*, 14, 460–464,
810 <https://doi.org/10.1038/s41561-021-00768-3>.

811 England, M., L. Polvani, and L. Sun, 2018: Contrasting the Antarctic and Arctic atmospheric
812 responses to projected sea ice loss in the late twenty-first century. *J. Clim.*, 31, 6353–
813 6370, <https://doi.org/10.1175/JCLI-D-17-0666.1>.

814 England, M. R., L. M. Polvani, and L. Sun, 2020a: Robust Arctic warming caused by
815 projected Antarctic sea ice loss. *Environ. Res. Letts.*, in press, 0–31,
816 <https://doi.org/10.1088/1748-9326/abaada>.

817 England, M. R., L. M. Polvani, L. Sun, and C. Deser, 2020b: Tropical climate responses to
818 projected Arctic and Antarctic sea-ice loss. *Nat. Geosci.*, 13, 275–281,
819 <https://doi.org/10.1038/s41561-020-0546-9>.

820 Eyring, V., S. Bony, G. A. Meehl, C. A. Senior, B. Stevens, R. J. Stouffer, and K. E. Taylor,
821 2016: Overview of the Coupled Model Intercomparison Project Phase 6 (CMIP6)
822 experimental design and organization. *Geosci. Model Dev.*, 9, 1937–1958,
823 <https://doi.org/10.5194/gmd-9-1937-2016>.

824 Farneti, R., and T. L. Delworth, 2010: The role of mesoscale eddies in the remote oceanic
825 response to altered Southern Hemisphere winds. *J. Phys. Oceanogr.*, 40, 2348–2354,
826 <https://doi.org/10.1175/2010JPO4480.1>.

827 Farneti, R., and T. L. Delworth, 2010, A. J. Rosati, S. M. Griffies, and F. Zeng, 2010: The
828 role of mesoscale eddies in the rectification of the Southern Ocean response to climate
829 change. *J. Phys. Oceanogr.*, 40, 1539–1557,
830 <https://doi.org/10.1175/2010JPO4353.1>. Flocco, D., D. L. Feltham, and A. K. Turner,
831 2010: Incorporation of a physically based melt pond scheme into the sea ice component
832 of a climate model. *J. Geophys. Res. Ocean.*, 115, 1–14,
833 <https://doi.org/10.1029/2009JC005568>.

834 Hunke, E. C., W. H. Lipscomb, A. K Turner, N. Jeffery and S. Elliott. 2015: CICE: the Los
835 Alamos Sea ice Model Documentation and Software User's Manual Version 5.1, LA-
836 CC-06-012, Los Alamos National Laboratory, Los Alamos, NM, 2015.

837 Kidston, J., A. S. Taschetto, D. W. J. Thompson, and M. H. England, 2011: The influence of
838 Southern Hemisphere sea-ice extent on the latitude of the mid-latitude jet stream.
839 *Geophys. Res. Lett.*, 38, 1–5, <https://doi.org/10.1029/2011GL048056>.

840 Kim, B. M., S. W. Son, S. K. Min, J. H. Jeong, S. J. Kim, X. Zhang, T. Shim, and J. H. Yoon,
841 2014: Weakening of the stratospheric polar vortex by Arctic sea-ice loss. *Nat. Commun.*,
842 5, 1–8, <https://doi.org/10.1038/ncomms5646>.

843 Kuhlbrodt, T., and Coauthors, 2018: The Low-Resolution Version of HadGEM3 GC3.1:
844 Development and Evaluation for Global Climate. *J. Adv. Model. Earth Syst.*, 10, 2865–
845 2888, <https://doi.org/10.1029/2018MS001370>.

846 Laliberté, F., and P. J. Kushner, 2013: Isentropic constraints by midlatitude surface warming
847 on the Arctic midtroposphere. *Geophys. Res. Lett.*, 40, 606–611,
848 <https://doi.org/10.1029/2012GL054306>.

849 Liu, J., and J. A. Curry, 2010: Accelerated warming of the Southern Ocean and its impacts on
850 the hydrological cycle and sea ice. *Proc. Natl. Acad. Sci. U. S. A.*, 107, 14987–14992,
851 <https://doi.org/10.1073/pnas.1003336107>.

852 Ludescher, J., N. Yuan, and A. Bunde, 2018: Detecting the statistical significance of the
853 trends in the Antarctic sea ice extent: an indication for a turning point. *Clim. Dyn.*, 53,
854 237–244, <https://doi.org/10.1007/s00382-018-4579-3>.

855 Mackie, S., I. J. Smith, J. K. Ridley, D. P. Stevens, and P. J. Langhorne, 2020: Climate
856 response to increasing antarctic iceberg and ice shelf melt. *J. Clim.*, 33, 8917–8938,
857 <https://doi.org/10.1175/JCLI-D-19-0881.1>.

858 McCrystall, M. R., J. S. Hosking, I. P. White, and A. C. Maycock, 2020: The Impact of
859 Changes in Tropical Sea Surface Temperatures over 1979–2012 on Northern Hemisphere
860 High-Latitude Climate. *J. Clim.*, 33, 5103–5121, <https://doi.org/10.1175/jcli-d-19-0456.1>.

861 Meehl, G. A., J. M. Arblaster, C. T. Y. Chung, M. M. Holland, A. DuVivier, L. Thompson,
862 D. Yang, and C. M. Bitz, 2019: Sustained ocean changes contributed to sudden Antarctic

863 sea ice retreat in late 2016. *Nat. Commun.*, 10, 14, [https://doi.org/10.1038/s41467-018-](https://doi.org/10.1038/s41467-018-07865-9)
864 07865-9.

865 Menary, M. B., and Coauthors, 2018: Preindustrial Control Simulations With HadGEM3-
866 GC3.1 for CMIP6. *J. Adv. Model. Earth Syst.*, 10, 3049–3075,
867 <https://doi.org/10.1029/2018MS001495>.

868 Menéndez, C. G., V. Serafini, and H. Le Treut, 1999: The effect of sea-ice on the transient
869 atmospheric eddies of the Southern Hemisphere. *Clim. Dyn.*, 15, 659–671,
870 <https://doi.org/10.1007/s003820050308>.

871 Meredith, M., M. Sommerkorn, S. Cassotta, C. Derksen, A. Ekaykin, A. Hollowed, G.
872 Kofinas, A. Mackintosh, J. Melbourne-Thomas, M.M.C. Muelbert, G. Ottersen, H.
873 Pritchard, and E.A.G. Schuur, 2019: Polar Regions. In: *IPCC Special Report on the*
874 *Ocean and Cryosphere in a Changing Climate*. IPCC, 3, S129–S131,
875 [https://doi.org/10.1016/S1366-7017\(01\)00066-6](https://doi.org/10.1016/S1366-7017(01)00066-6).

876 Munday, D. R., H. L. Johnson, and D. P. Marshall, 2013: Eddy saturation of equilibrated
877 circumpolar currents. *J. Phys. Oceanogr.*, 43, 507–532, [https://doi.org/10.1175/JPO-D-12-](https://doi.org/10.1175/JPO-D-12-095.1)
878 095.1.

879 Oudar, T., E. Sanchez-Gomez, F. Chauvin, J. Cattiaux, L. Terray, and C. Cassou, 2017:
880 Respective roles of direct GHG radiative forcing and induced Arctic sea ice loss on the
881 Northern Hemisphere atmospheric circulation. *Clim. Dyn.*, 0, 1–21,
882 <https://doi.org/10.1007/s00382-017-3541-0>.

883 Parkinson, C. L., 2019: A 40-y record reveals gradual Antarctic sea ice increases followed by
884 decreases at rates far exceeding the rates seen in the Arctic. *Proc. Natl. Acad. Sci.*,
885 201906556, <https://doi.org/10.1073/pnas.1906556116>.

886 Peings, Y., and G. Magnusdottir, 2014: Response of the wintertime northern hemisphere
887 atmospheric circulation to current and projected arctic sea ice decline: A numerical study
888 with CAM5. *J. Clim.*, 27, 244–264, <https://doi.org/10.1175/JCLI-D-13-00272.1>.

889 Polvani, L. M., D. W. Waugh, G. J. P. Correa, and S. W. Son, 2011: Stratospheric ozone
890 depletion: The main driver of twentieth-century atmospheric circulation changes in the
891 Southern Hemisphere. *J. Clim.*, 24, 795–812, <https://doi.org/10.1175/2010JCLI3772.1>.

892 Hallberg, R., and A. Gnanadesikan, 2006: The Role of Eddies in Determining the Structure
893 and Response of the Wind-Driven Southern Hemisphere Overturning: Results from the
894 Modeling Eddies in the Southern Ocean (MESO) Project. *J. Phys. Oceanogr.*, 36, 2232–
895 2252.

896 Raphael, M. N., W. Hobbs, and I. Wainer, 2011: The effect of Antarctic sea ice on the
897 Southern Hemisphere atmosphere during the southern summer. *Clim. Dyn.*, 36, 1403–
898 1417, <https://doi.org/10.1007/s00382-010-0892-1>.

899 Raphael, M.N., and M.S. Handcock, 2022: A new record minimum for Antarctic sea ice. *Nat*
900 *Rev Earth Environ* . <https://doi.org/10.1038/s43017-022-00281-0>

901 Ridley, J. K., E. W. Blockley, A. B. Keen, J. G. L. Rae, A. E. West, and D. Schroeder, 2018:
902 The sea ice model component of HadGEM3-GC3.1. *Geosci. Model Dev.*, 11, 713–723,
903 <https://doi.org/10.5194/gmd-11-713-2018>.

904 Roach, L. A., and Coauthors, 2020: Antarctic Sea Ice Area in CMIP6. *Geophys. Res. Lett.*,
905 47, 1–10, <https://doi.org/10.1029/2019GL086729>.

906 Schlosser, E., F. A. Haumann, M. N. Raphael, F. Alexander Haumann, and M. N. Raphael,
907 2017: Atmospheric influences on the anomalous 2016 Antarctic sea ice decay. *Cryosph.*
908 *Discuss.*, 13, 1–31, <https://doi.org/10.5194/tc-2017-192>.

909 Scott, F., and D. L. Feltham, 2010: A model of the three-dimensional evolution of Arctic melt
910 ponds on first-year and multiyear sea ice. *J. Geophys. Res. Ocean.*, 115, 1–37,
911 <https://doi.org/10.1029/2010JC006156>.

912 Screen, J. A., and I. Simmonds, 2013: Exploring links between Arctic amplification and mid-
913 latitude weather. *Geophys. Res. Lett.*, 40, 959–964, <https://doi.org/10.1002/grl.50174>.

914 Screen, J. A., and I. Simmonds, C. Deser, and R. Tomas, 2013: The atmospheric response to
915 three decades of observed arctic sea ice loss. *J. Clim.*, 26, 1230–1248,
916 <https://doi.org/10.1175/JCLI-D-12-00063.1>.

917 Screen, J. A., and Coauthors, 2018a: Consistency and discrepancy in the atmospheric
918 response to Arctic sea-ice loss across climate models. *Nat. Geosci.*, 11, 155–163,
919 <https://doi.org/10.1038/s41561-018-0059-y>.

920 Screen, J. A., T. J. Bracegirdle, and I. Simmonds, 2018b: Polar Climate Change as Manifest
921 in Atmospheric Circulation. *Curr. Clim. Chang. Reports*, 4, 383–395,
922 <https://doi.org/10.1007/s40641-018-0111-4>.

923 Shi, J. R., L. D. Talley, S. P. Xie, Q. Peng, and W. Liu, 2021: Ocean warming and
924 accelerating Southern Ocean zonal flow. *Nat. Clim. Chang.*, 11, 1090–1097,
925 <https://doi.org/10.1038/s41558-021-01212-5>.

926 Simpson, I. R., K. A. McKinnon, F. V. Davenport, M. Tingley, F. Lehner, A. Al Fahad, and
927 D. Chen, 2021: Emergent constraints on the large-scale atmospheric circulation and
928 regional hydroclimate: Do they still work in CMIP6 and how much can they actually
929 constrain the future? *J. Clim.*, 34, 6355–6377, <https://doi.org/10.1175/JCLI-D-21-0055.1>.

930 Singh, H. A., L. M. Polvani, and P. J. Rasch, 2019: Antarctic Sea Ice Expansion, Driven by
931 Internal Variability , in the Presence of Increasing Atmospheric.
932 <https://doi.org/10.1029/2019GL083758>.

933 Smith, D. M., N. J. Dunstone, A. A. Scaife, E. K. Fiedler, D. Copey, and S. C. Hardiman,
934 2017: Atmospheric response to Arctic and Antarctic sea ice: The importance of ocean-
935 atmosphere coupling and the background state. *J. Clim.*, 30, 4547–4565,
936 <https://doi.org/10.1175/JCLI-D-16-0564.1>.

937 Smith, D. M., and Coauthors, 2018: The Polar Amplification Model Intercomparison Project
938 (PAMIP) contribution to CMIP6: investigating the causes and consequences of polar
939 amplification. *Geosci. Model Dev. Discuss.*, 1–42, <https://doi.org/10.5194/gmd-2018-82>.

940 Storkey, D., and Coauthors, 2018: UK Global Ocean GO6 and GO7: A traceable hierarchy of
941 model resolutions. *Geosci. Model Dev.*, 11, 3187–3213, <https://doi.org/10.5194/gmd-11-3187-2018>.

943 Stuecker, M. F., C. M. Bitz, and K. C. Armour, 2017: Conditions leading to the
944 unprecedented low Antarctic sea ice extent during the 2016 austral spring season.
945 *Geophys. Res. Lett.*, 1–12, <https://doi.org/10.1002/2017GL074691>.

946 Sun, L., C. Deser, R. A. Tomas, and M. Alexander, 2020: Global Coupled Climate Response
947 to Polar Sea Ice Loss: Evaluating the Effectiveness of Different Ice-Constraining
948 Approaches. *Geophys. Res. Lett.*, 47, <https://doi.org/10.1029/2019GL085788>..

949 Taylor, K. E., R. J. Stouffer, and G. A. Meehl, 2012: An overview of CMIP5 and the
950 experiment design. *Bull. Am. Meteorol. Soc.*, 93, 485–498,
951 <https://doi.org/10.1175/BAMS-D-11-00094.1>.

952 Tomas, R. A., C. Deser, and L. Sun, 2016: The role of ocean heat transport in the global
953 climate response to projected arctic sea ice loss. *J. Clim.*, 29, 6841–6859,
954 <https://doi.org/10.1175/JCLI-D-15-0651.1>.

955 Turner, J., 2004: The El Niño-Southern Oscillation and Antarctica. *Int. J. Climatol.*, 24, 1–31,
956 <https://doi.org/10.1002/joc.965>.

957 Turner, J., and Coauthors, 2009: Non-annular atmospheric circulation change induced by
958 stratospheric ozone depletion and its role in the recent increase of Antarctic sea ice extent.
959 *Geophys. Res. Lett.*, 36, 1–5, <https://doi.org/10.1029/2009GL037524>.

960 Turner, J., T. Phillips, G. J. Marshall, J. S. Hosking, J. O. Pope, T. J. Bracegirdle, and P.
961 Deb, 2017: Unprecedented springtime retreat of Antarctic sea ice in 2016. *Geophys. Res.*
962 *Lett.*, 44, 6868–6875, <https://doi.org/10.1002/2017GL073656>.

963 Turner, J., and Coauthors, 2020: Recent Decrease of Summer Sea Ice in the Weddell Sea,
964 Antarctica. *Geophys. Res. Lett.*, 47, <https://doi.org/10.1029/2020GL087127>.

965 Vavrus, S. J., 2018: The Influence of Arctic Amplification on Mid-latitude Weather and
966 Climate. *Curr. Clim. Chang. Reports*, 4, 238–249, [https://doi.org/10.1007/s40641-018-](https://doi.org/10.1007/s40641-018-0105-2)
967 [0105-2](https://doi.org/10.1007/s40641-018-0105-2).

968 Walters, D., and Coauthors, 2017: The Met Office Unified Model Global Atmosphere 7.0/7.1
969 and JULES Global Land 7.0 configurations. *Geosci. Model Dev.*, 12, 1909–1963,
970 <https://doi.org/10.5194/gmd-12-1909-2019>.

971 Wang, Z., J. Turner, Y. Wu, and C. Liu, 2019: Rapid decline of total Antarctic sea ice extent
972 during 2014–16 controlled by wind-driven sea ice drift. *J. Clim.*, 32, 5381–5395,
973 <https://doi.org/10.1175/JCLI-D-18-0635.1>.

974 Williams, K. D., and Coauthors, 2017: The Met Office Global Coupled Model 3.0 and 3.1
975 (GC3.0 and GC3.1) Configurations. *J. Adv. Model. Earth Syst.*, 10, 357–380,
976 <https://doi.org/10.1002/2017MS001115>.

- 977 Yuan, X., M. R. Kaplan, and M. A. Cane, 2018: The interconnected global climate system-a
978 review of tropical-polar teleconnections. *J. Clim.*, 31, 5765–5792,
979 <https://doi.org/10.1175/JCLI-D-16-0637.1>.
- 980 Zappa, G., F. Pithan, and T. G. Shepherd, 2018a: Multimodel Evidence for an Atmospheric
981 Circulation Response to Arctic Sea Ice Loss in the CMIP5 Future Projections. *Geophys.*
982 *Res. Lett.*, 45, 1011–1019, <https://doi.org/10.1002/2017GL076096>.